

Optimizing Highway Traffic Flow in Mixed Autonomy: A Multiagent Truncated Rollout Approach

Lu Liu, Chi Xie, and Xi Xiong *

Abstract

The development of connected and autonomous vehicles (CAVs) offers substantial opportunities to enhance traffic efficiency. However, in mixed autonomy environments where CAVs coexist with human-driven vehicles (HDVs), achieving efficient coordination among CAVs remains challenging due to heterogeneous driving behaviors. To address this, this paper proposes a multiagent truncated rollout approach that enhances CAV speed coordination to improve highway throughput while reducing computational overhead. In this approach, a traffic density evolution equation is formulated that comprehensively accounts for the presence or absence of CAVs, and a distributed coordination control framework is established accordingly. By incorporating kinematic information from neighbor agents and employing an agent-by-agent sequential solution mechanism, our method enables explicit cooperation among CAVs. Furthermore, we introduce a truncated rollout scheme that adaptively shortens the optimization horizon based on the evaluation of control sequences. This significantly reduces the time complexity, thereby improving real-time performance and scalability. Theoretical analysis provides rigorous guarantees on the stability and performance improvement of the system. Simulations conducted on real-world bottleneck scenarios demonstrate that, in large-scale mixed traffic flows, the proposed method outperforms conventional model predictive control methods by reducing both the average travel time in the bottleneck area and overall computational time, highlighting its strong potential for practical deployment.

Keywords: Connected and autonomous vehicles, traffic flow optimization, multiagent rollout, model predictive control.

1 Introduction

Connected and autonomous vehicles (CAVs), enabled by vehicle-to-vehicle (V2V) and vehicle-to-infrastructure (V2I) communication technologies as well as high-precision control systems,

*The authors are with the the Key Laboratory of Road and Traffic Engineering, Ministry of Education, Tongji University, Shanghai, China. (emails: lulu0720@tongji.edu.cn, chi.xie@tongji.edu.cn, xi_xiong@tongji.edu.cn)

provide the technological foundation for improving traffic efficiency and reducing accident risks [26]. However, the replacement of human-driven vehicles (HDVs) by CAVs is a gradual process, and a mixed autonomy traffic environment will persist for the foreseeable future [20]. In such environments, the fundamental behavioral differences between CAVs and HDVs significantly limit the effectiveness of CAV coordination. This issue becomes particularly critical in lane-merging bottleneck areas, where the traffic outflow initially increases linearly with inflow, but drops sharply once vehicle density exceeds a critical threshold, triggering queue formation and propagation at the merging point [9]. Conventional approaches such as signal control and ramp metering often fail to handle dynamic traffic fluctuations effectively [16, 18], while roadway expansion is limited by high construction costs and the risk of induced demand [1]. Although existing studies have shown that CAVs can improve bottleneck throughput via speed control [31], several core limitations remain under mixed traffic conditions. These include the lack of modeling for interactions between HDVs and CAVs, the absence of a systematic heterogeneous decision-making framework, and the inadequacy of control strategies in real-time performance [8, 32, 43].

To bridge these gaps, we propose a distributed framework for CAVs in mixed autonomy, aiming to enhance traffic efficiency by coordinating their driving behaviors. Specifically, we consider a three-to-two lane merging scenario as illustrated in Fig. 1, where white and blue vehicles denote HDVs and CAVs, respectively. A coordination zone is established upstream of the bottleneck, within which CAVs can perceive traffic state information through onboard sensors such as radar and cameras. Leveraging vehicle-to-vehicle communication systems, these CAVs collaborate to decide whether to accelerate through the bottleneck or decelerate to delay the entry of the following vehicles. This CAV-centered control approach not only reduces reliance on traditional infrastructure upgrades but also adapts flexibly to dynamic traffic flow variations. Moreover, by incorporating a sequential optimization mechanism and an advanced truncated algorithm, the coordination and computational efficiency of CAVs are further enhanced. While lane-changing constitutes a potential action, it may introduce significant complexity [39] and is therefore deferred to future research. In this study, we focus solely on the longitudinal speed control of CAVs. Meanwhile, we assume that communication among CAVs is instantaneous, an assumption widely adopted in many previous multiagent studies [12, 40].

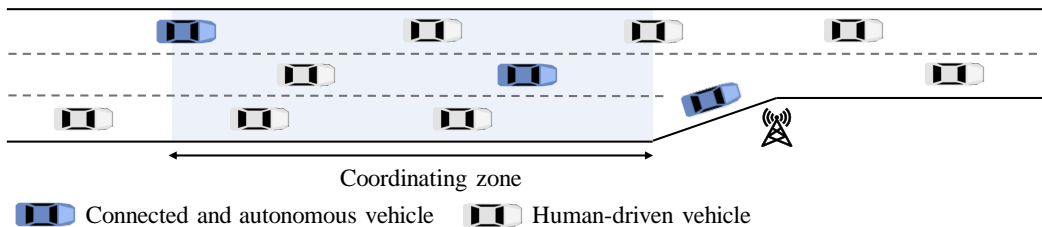


Figure 1: Illustration of CAV coordination in mixed autonomy at a highway bottleneck.

Most existing studies on coordinating CAVs to mitigate congestion focus on homogeneous traffic flow [29, 44]. In the coordinated control of mixed traffic flow, existing modeling approaches still face theoretical challenges: (1) Although microscopic traffic flow models can describe individual vehicle dynamics, they struggle to address coordinated decision-making

of CAVs [14]; (2) Macroscopic models leveraging flow-density-speed relationships achieve computational efficiency in large-scale systems but fail to account for heterogeneous behaviors between HDVs and CAVs [34]. To integrate the advantages of both microscopic and macroscopic models, Liard et al. [22] proposed a coupled model that uses partial differential equations (PDEs) to describe the evolution of traffic density and ordinary differential equations (ODEs) to model the trajectories of CAVs, commonly referred to as a PDE-ODE coupled model. They also proved the existence of solutions to the coupled system. Based on this framework, Zhang et al. [48] designed an adaptive observer to achieve high-accuracy traffic state estimation. Daini et al. [11] further demonstrated that the PDE-ODE model, which takes CAV speed as the control variable, can effectively capture multiagent coordination and achieve superior traffic flow control. In our study, this PDE-ODE coupled model is also employed to investigate the cooperative control of CAVs in heterogeneous traffic flow. However, the solving of PDEs usually involves high computational complexity, and thus there is a large computational burden on the model in practical applications. The cell transmission model (CTM) effectively bridges the scale gap between microscopic CAV trajectories and macroscopic traffic evolution, serving as a key method for discretizing continuum traffic models [33, 54]. Leveraging this, Qiu and Du [35] developed a model predictive control (MPC) for online motion planning of CAVs. By minimizing objective functions over rolling horizons, the MPC implementation achieved global optimality in speed adjustments [46]. Nevertheless, due to the exponential growth in computational costs, the traditional MPC faces dimensional difficulties in complex traffic flow [37, 50]. Distributed model predictive control (DMPC) addresses this by decomposing large-scale systems into subsystems with parallelized optimization [15]. However, since subsystems only exchange information from previous iterations, DMPC yields suboptimal solutions relative to centralized MPC [24]. Additionally, the DMPC method faces challenges in stability analysis [51].

The rolling optimization mechanism in traditional MPC, which employs an explicit system model to predict state trajectories over a finite time horizon, is analogous to the rollout in reinforcement learning (RL) [41]. The difference is that in RL-based multiagent control, CAVs acquire traffic state information through interaction with the environment and continuously refine their policies by training on state-action-reward outcomes [23, 52]. Despite their successes in traffic flow control, RL methods exhibit limitations in large-scale systems, including high data requirements, environmental non-stationarity, and low training efficiency [2]. Moreover, their computational complexity tends to grow exponentially with system scale [6]. To address these, some researchers have leveraged the multiagent advantage decomposition theorem to reformulate the joint policy search problem as a sequential decision-making process, thereby reducing the complexity to linear in the number of agents [19, 42, 49]. However, these sequential optimization methods typically rely on a full-horizon rollout process, which introduces additional computational overhead. Bhattacharya et al. [7] introduced a multiagent truncated rollout technique that replaces full-horizon state tracking with finite-step lookahead simulations and terminal cost approximations. This locally sequential optimization algorithm balances performance and computational efficiency, providing a novel control paradigm for large-scale multiagent systems [21]. Although a similar idea, known as the adaptive receding horizon approach [27], has been explored in traditional MPC methods to improve computational efficiency by adjusting the dimension of the optimization variables, this approach alters the length of the control sequence, potentially compromising control

performance.

In this study, we propose a multiagent truncated rollout approach that integrates the strengths of MPC and truncated rollout. We begin with a PDE-ODE coupled model [22] to describe mixed traffic flow dynamics, and construct a system-level density evolution equation based on the CTM [33], which characterizes the evolution of cell densities in the presence and absence of CAVs. Leveraging this equation, we develop a distributed optimization framework that incorporates the control information of all CAVs. Within this framework, each CAV is equipped with an independent MPC controller, which obtains real-time traffic states and trajectory information of other CAVs through communication infrastructure and onboard sensors, enabling reasonable prediction of future traffic states and optimal decision-making. To promote explicit cooperation among CAVs and overcome the lack of coordination in conventional DMPC, we design an agent-by-agent sequential optimization mechanism. Each CAV can fully take into account the latest control information of others and iteratively refine its own actions, gradually steering the system toward joint optimality. Furthermore, to enhance computational efficiency during the optimization process, we incorporate the truncated rollout method. By estimating the upper and lower bounds of the objective value and adaptively shortening the optimization horizon, this method reduces the problem scale and avoids the computational burden typically encountered in large-scale systems.

We systematically analyze the policy improvement of the multiagent truncated rollout method from the perspectives of sequential decision-making and truncated optimization, and rigorously prove the input-to-state stability of each CAV subsystem. Although global optimality is not the direct objective of this work, our analysis guarantees that the proposed method enables the control policy to progressively approach the global optimum, while the system state ultimately converges to an invariant set. In addition, we design an optimized decision-ordering strategy for CAVs at each time step, and derive upper and lower bounds of the objective function to maximize system-level performance. The multiagent truncated rollout algorithm is also presented, and a time complexity analysis is conducted, further demonstrating its superior computational time reduction compared to conventional model predictive control methods. We select a bottleneck segment of the Shanghai Hujin Expressway as a test scenario to evaluate the control performance of CAVs under complex traffic conditions. Simulation results show that, in large-scale mixed traffic flow, the multiagent truncated rollout approach effectively coordinates the longitudinal behavior of CAVs, reduces vehicle travel time, and significantly lowers computational costs, demonstrating strong potential for real-world deployment.

The remainder of the paper is structured as follows: Section 2 introduces the coupled model characterizing mixed traffic flow dynamics and formulates the distributed control problem for CAVs. Section 3 presents the multiagent truncated rollout approach in detail, along with its performance analysis. Section 4 discusses the computational advantages of the proposed algorithm. Section 5 evaluates the effectiveness of the method through comparative simulation experiments. Finally, Section 6 concludes the paper and outlines several directions for future work.

2 Modeling and Formulation

This section introduces a fully coupled PDE-ODE model [22] to characterize the impact of CAVs on highway traffic. By discretizing the road segment using the cell transmission model (CTM), we derive the density evolution equations for individual road cells (Section 2.1). Furthermore, we establish a unified system density evolution equation that captures the dynamics of road cells both with and without the influence of CAVs, and formulate a distributed optimization problem in which each CAV acts as an independent actuator (Section 2.2).

2.1 Modeling

We utilize the classical Lighthill-Whitham-Richards (LWR) equation [36], a first-order macroscopic model, to describe the behavior of CAVs on highways and their impact on adjacent traffic. Specifically, the general evolution of traffic flow on a unidirectional road can be captured by a hyperbolic PDE [22],

$$\partial_t \rho + \partial_x f(\rho) = 0, \quad (1)$$

where $\rho = \rho_x^t \in [0, R)$ represents the traffic density at position $x \in \mathbb{R}$ at time $t \geq 0$, R is the jam density of the road. The flow function $f(\rho)$ is given by $f(\rho) = \rho v(\rho)$, where $v(\rho) = V(1 - \rho/R)$ and the constant V represents the maximum speed of vehicles. The $f(\rho)$ reaches its maximum value at $\rho_* = R/2$ [53].

The position of the CAV is represented by $y^t \in [0, L]$, and its trajectory can be described by the following ODE,

$$\partial_t y^t = \min \{u^t, v_*(\rho_{y_+}^t)\}, \quad (2)$$

where $L \in \mathbb{N}$ is the length of the road, $u^t \in U$ is the desired velocity of the CAV, $U = [u_{\min}, u_{\max}]$, and $\rho_{y_+}^t$ denotes the density value downstream of y^t . This formula indicates that the CAV can proceed at its desired speed if the downstream traffic is not congested, otherwise it will adjust to the downstream traffic speed.

By integrating Eq. (1) and Eq. (2), a fully coupled PDE-ODE model with multiple CAVs is developed,

$$\partial_t \rho_x^t + \partial_x f(\rho_x^t) = 0, \quad t > 0, x \in \mathbb{R}, \quad (3a)$$

$$\partial_t y_i^t = \min \{u_i^t, v(\rho_{y_{i+}}^t)\}, \quad t > 0, i \in \mathcal{I}^t, \quad (3b)$$

$$f(\rho_{y_i}^t) - \partial_t y_i^t \times \rho_{y_i}^t \leq \frac{\alpha R}{4V} (V - \partial_t y_i^t)^2, \quad t > 0, i \in \mathcal{I}^t, \quad (3c)$$

$$f(\rho_0^t) = f_{\text{in}}, \quad t > 0, \quad (3d)$$

$$f(\rho_L^t) = f_{\text{out}}, \quad t > 0, \quad (3e)$$

where $\mathcal{I}^t = \{0, 1, 2, \dots, I\}$ is the set of CAVs at time t , and $i \in \mathcal{I}^t$ is the index of the CAV. The parameter $\alpha \in (0, 1)$ indicates the reduction in road capacity due to the presence of the CAVs [10], and we set $\alpha = \frac{W-1}{W}$, where $W > 1$ denotes the number of lanes upstream of the merge point.

To solve the vehicle conservation equation, Eq. (3a) is discretized in both time and space. We set the system update interval as $\Delta t > 0$, and the length of the road cell $j \in \mathcal{J} = \{0, 1, \dots, J\}$ in the coordination zone is $\Delta x > 0$, where Δt and Δx satisfy the Courant-Friedrichs-Lewy (CFL) condition [47], $V\Delta t \leq 0.9\Delta x$. In addition, we define the center position of cell j as $x_j = (j + 1/2)\Delta x$, with the upstream and downstream boundaries given by $x_{j-1/2} = j\Delta x$ and $x_{j+1/2} = (j + 1)\Delta x$, respectively. Specifically, $x_{-1/2} = 0$ and $x_{J+1/2} = L$. At each time step $k \in \{1, 2, \dots\}$, the density ρ_j^k of each cell j , bounded by $\mathcal{D} = [0, \rho_{\max}]$, is updated using the supply-demand equation [17],

$$\rho_j^{k+1} = \rho_j^k - \frac{\Delta t}{\Delta x} \left(F_{j+\frac{1}{2}}^k - F_{j-\frac{1}{2}}^k \right), \quad (4a)$$

$$F_{j+\frac{1}{2}}^k = \min \{ D(\rho_j^k), S(\rho_{j+1}^k) \}, \quad (4b)$$

$$F_{j-\frac{1}{2}}^k = \min \{ D(\rho_{j-1}^k), S(\rho_j^k) \}, \quad (4c)$$

$$D(\rho) = f(\min \{ \rho, \rho_* \}), \quad (4d)$$

$$S(\rho) = f(\max \{ \rho, \rho_* \}). \quad (4e)$$

This equation is governed by the upstream flow $F_{j-\frac{1}{2}}^k$ and the downstream flow $F_{j+\frac{1}{2}}^k$. And the $F_{-1/2}^k$ and $F_{J+1/2}^k$ are calculated using $D(\rho_{-1}^k) = f_{\text{in}}^k$ and $S(\rho_{J+1}^k) = f_{\text{out}}^k$, where $\rho_{-1}^k = f_{\text{in}}^k/V$ and $\rho_{J+1}^k = f_{\text{out}}^k/V$.

2.2 Problem Definition

Considering the scenario depicted in Fig. 1, CAVs acquire road density states and the action information of other CAVs through infrastructure communication without delay. Then, before entering the bottleneck, they predict future road states and execute longitudinal control actions to regulate the subsequent entry of HDVs, thereby alleviating congestion and improving road throughput.

However, in mixed autonomy traffic flow, the speed control of CAVs may introduce discontinuities in the surrounding traffic density. To investigate this problem, at time step k , we consider the upstream and downstream densities of the cell j' where CAV $i \in \mathcal{I}^k$ is located as Riemann-type initial reference. When the vehicle moves at the desired speed u_i^k and the constraint (3c) is not satisfied (such CAVs are referred to as controlled CAVs), its upstream and downstream densities are updated to $\hat{\rho}_{j'-\frac{1}{2}}^k(u_i)$ and $\check{\rho}_{j'+\frac{1}{2}}^k(u_i)$ respectively [10]. These updated values simulate the congestion effect induced by the controlled CAV. The flow between the cell j' and $j' - 1$, $j' + 1$ can be reconstructed as,

$$F_{j'-\frac{1}{2}}^k = \min \left\{ D(\rho_{j'-1}^k), S(\hat{\rho}_{j'-\frac{1}{2}}^k(u_i)) \right\}, \quad (5)$$

$$\Delta t \times F_{j'+\frac{1}{2}}^k = \min \{ \Delta t_i^k, \Delta t \} f(\check{\rho}_{j'+\frac{1}{2}}^k(u_i)) + \max \{ \Delta t - \Delta t_i^k, 0 \} f(\hat{\rho}_{j'+\frac{1}{2}}^k(u_i)), \quad (6)$$

where Δt_i^k represents the time required for CAV i to reach the downstream $x_{j'+1/2}$,

$$\Delta t_i^k = \frac{1 - d_i^k}{u_i^k} \Delta x, \quad d_i^k = \frac{\rho_{j'-\frac{1}{2}}^k - \hat{\rho}_{j'-\frac{1}{2}}^k(u_i)}{\check{\rho}_{j'+\frac{1}{2}}^k(u_i) - \hat{\rho}_{j'-\frac{1}{2}}^k(u_i)}.$$

This reconstruction process of density and flow directly reflects the constraint (3c), and therefore, it will not be restated explicitly in the subsequent discussion. When multiple CAVs are in the same cell, they are checked sequentially for compliance with constraint (3c). If there is more than one moving bottleneck, the controlled CAV closest to the downstream is used for flow reconstruction, as it has a greater impact on the traffic flow.

Accordingly, for each time step k , the manner in which cell densities are updated within the multiagent system varies depending on whether a CAV acts as a moving bottleneck, and is formally described as follows,

$$\begin{aligned}\rho_j^{k+1} &= \rho_j^k + f_1(\rho_{j-1}^k, \rho_j^k, \rho_{j+1}^k), & \forall i \in \mathcal{I}^k, y_i^k \notin [j\Delta x, (j+1)\Delta x) \text{ or } u_i^k = 0 \text{ or } \neg\Gamma_{i,j}^k, \\ \rho_j^{k+1} &= \rho_j^k + f_2(\rho_{j-1}^k, \rho_j^k) + f_3(u_i^k), & \exists i \in \mathcal{I}^k, y_i^k \in [j\Delta x, (j+1)\Delta x), u_i^k \neq 0 \text{ and } \Gamma_{i,j}^k,\end{aligned}$$

where f_1, f_2, f_3 are all nonlinear functions computed from the flow at the cell interfaces and the CAV actions in Eq. (4). Condition $\Gamma_{i,j}^k := \gamma_1(\rho_j^k) < u_i^k < \gamma_2(\rho_j^k)$ checks if the control action of CAV i is within the range defined by $\gamma_1(\rho_j^k)$ and $\gamma_2(\rho_j^k)$, which violates the constraint (3c). The condition $\neg\Gamma_{i,j}^k := u_i^k \leq \gamma_1(\rho_j^k)$ or $u_i^k \geq \gamma_2(\rho_j^k)$ means that CAV i is not acting as a moving bottleneck. The detailed derivations are provided in Appendix A and Appendix B.

To unify the description of density transitions for different scenarios, we define the vector $\mathbf{O}^k = [o_0^k, o_1^k, \dots, o_J^k]^T \in \mathbb{R}^{J+1}$, where $o_j^k = 1$ indicates that cell j contains a CAV whose action remains within the maximum allowable downstream limit but does not satisfy the maximum flow reduction constraint at time step k , and $o_j^k = 0$ otherwise. The control action of CAV i is also transformed into a vector $\mathbf{u}_i^k = [u_{i,0}^k, u_{i,1}^k, \dots, u_{i,J}^k]^T \in \mathbb{R}^{J+1}$, with non-zero input only in the cell occupied by this CAV. The state transition equation of the overall system can be modeled as,

$$\boldsymbol{\rho}^{k+1} = \boldsymbol{\rho}^k + \mathbf{A}^k \mathbf{O}^k + \mathbf{B}^k + \mathbf{C}_{\mathbf{u}}^k, \quad (7)$$

where $\boldsymbol{\rho}^k = [\rho_0^k, \rho_1^k, \dots, \rho_J^k]^T \in \mathbb{R}^{J+1}$ represents the density state of the whole road segment. The matrices $\mathbf{A}^k \in \mathbb{R}^{(J+1) \times (J+1)}$, $\mathbf{B}^k \in \mathbb{R}^{J+1}$, and $\mathbf{C}_{\mathbf{u}}^k \in \mathbb{R}^{J+1}$ are calculated as following,

$$\begin{aligned}\mathbf{A}^k &= \text{diag}(A_{0,0}^k, A_{1,1}^k, \dots, A_{J,J}^k), \quad A_{j,j}^k = f_2(\rho_{j-1}^k, \rho_j^k) - f_1(\rho_{j-1}^k, \rho_j^k, \rho_{j+1}^k), \\ \mathbf{B}^k &= \left[f_1(\rho_{-1}^k, \rho_0^k, \rho_1^k), f_1(\rho_0^k, \rho_1^k, \rho_2^k), \dots, f_1(\rho_{J-1}^k, \rho_J^k, \rho_{J+1}^k) \right]^T, \\ \mathbf{C}_{\mathbf{u}}^k &= [C_{\mathbf{u},0}^k, C_{\mathbf{u},1}^k, \dots, C_{\mathbf{u},J}^k]^T, \quad C_{\mathbf{u},j}^k = \begin{cases} f_3(u_{i_j^*,j}^k), & o_j^k = 1, \\ 0, & o_j^k = 0, \end{cases} \\ o_j^k &= \begin{cases} 1, & \exists i \in \mathcal{I}^k, y_i^k \in [j\Delta x, (j+1)\Delta x), u_{i,j}^k \neq 0 \text{ and } \Gamma_{i,j}^k, \\ 0, & \forall i \in \mathcal{I}^k, y_i^k \notin [j\Delta x, (j+1)\Delta x) \text{ or } u_{i,j}^k = 0 \text{ or } \neg\Gamma_{i,j}^k, \end{cases} \\ i_j^* &= \min \{i \in \mathcal{I}^k \mid y_i^k \in [j\Delta x, (j+1)\Delta x), u_{i,j}^k \neq 0, \Gamma_{i,j}^k\}, \end{aligned}$$

where i_j^* denotes the index of the CAV that is located at cell j , closest to the downstream and is the moving bottleneck.

The position $y_i \in [0, L]$ of each CAV i is updated as,

$$y_i^{k+1} = y_i^k + \min \{ \max(\mathbf{u}_i^k), v(\rho_{y_i+}^k) \} \Delta t.$$

Based on the aforementioned state transition equations, we formulate a distributed co-operative control problem for each CAV, where the traffic density of road cells is treated as the state variable, the speed of the CAV serves as the control input, and the objective is to minimize the total travel time of all vehicles within the controlled road segment. Taking the subsystem of CAV i as an example, at sampling time step k , both the prediction horizon and control horizon are set to $N > 0$, and the perceived traffic state is denoted by $\rho_i^k = \boldsymbol{\rho}^k \in \mathcal{D}$, where $\mathcal{D} \in \mathbb{R}^{J+1}$ and each component $\rho_{i,j}^k = \rho_j^k \in \mathcal{D}$, $j \in \mathcal{J}$. The objective function, denoted by,

$$J_i(\boldsymbol{\xi}_i^k, \boldsymbol{\mu}_i^k) = \sum_{t=0}^{N-1} \sum_{j=0}^J \rho_{i,j}^{k+t} \Delta t \Delta x,$$

characterizes the total time spent by all vehicles through the evolution of traffic density across road cells over time. As a system-level cost, it enables each agent to independently optimize its local control actions while collectively contributing to the maximization of overall traffic efficiency. The $\boldsymbol{\mu}_i^k = [\mathbf{u}_i^{k+0}, \mathbf{u}_i^{k+1}, \dots, \mathbf{u}_i^{k+N-1}] \in \mathbb{R}^{(J+1) \times N}$ represents the predicted inputs applied by CAV i from time step $k\Delta t$ to $(k+N-1)\Delta t$, and $\boldsymbol{\xi}_i^k = [\boldsymbol{\rho}_i^{k+1}, \boldsymbol{\rho}_i^{k+2}, \dots, \boldsymbol{\rho}_i^{k+N}] \in \mathbb{R}^{(J+1) \times N}$ denotes the corresponding predicted evolution of traffic states. The prediction model employed during optimization is expressed as,

$$\boldsymbol{\rho}_i^{k+1} = \boldsymbol{\rho}_i^k + \mathbf{A}_i^k \mathbf{O}_i^k + \mathbf{B}_i^k + \mathbf{C}_{\mathbf{u},i}^k.$$

Utilizing matrix $\mathbf{C}_{\mathbf{u},i}^k$, CAV i can explicitly account for the control actions of other agents j , thereby ensuring coordination among control actions.

3 Optimal Policy with Multiagent Truncated Rollout

In this section, we introduce the framework of the multiagent truncated rollout (Section 3.1) and present its enhancement in cost performance (Section 3.2). Additionally, we conduct a stability analysis of the proposed approach (Section 3.3).

3.1 Framework of Multiagent Truncated Rollout

As a special case of the rollout, model predictive control (MPC) enables online prediction of future states and optimization of vehicle actions [46]. Leveraging this property, in this section, we propose a multiagent truncated rollout approach based on the distributed model predictive control (DMPC) framework. By integrating an agent-by-agent sequential optimization mechanism with the truncated rollout approach that shortens the optimization horizon, the proposed method enhances optimization in both spatial and temporal dimensions while alleviating computational burden, thereby achieving more efficient and effective control of mixed traffic flow.

3.1.1 Multiagent Model Predictive Control

In the multiagent truncated rollout method, each CAV is equipped with its own controller. These controllers receive driving information from all other CAVs, predict the evolution of traffic states, and independently solve an optimization problem to obtain an optimal control sequence. Specifically, for each CAV $i \in \mathcal{I}^k$, the travel cost optimization problem can be formulated as,

$$\boldsymbol{\mu}_i^{k*} = \arg \min_{\boldsymbol{\mu}_i^k} J_i(\boldsymbol{\xi}_i^k, \boldsymbol{\mu}_i^k), \quad (8a)$$

$$\text{s.t. } \boldsymbol{\rho}_i^{k+t+1} = \boldsymbol{\rho}_i^{k+t} + \mathbf{A}_i^{k+t} \mathbf{O}_i^{k+t} + \mathbf{B}_i^{k+t} + \mathbf{C}_{\mathbf{u},i}^{k+t}, \quad (8b)$$

$$y_{i'}^{k+t+1} = y_{i'}^{k+t} + \min \left\{ \max(\mathbf{u}_{i'}^{k+t}), v(\rho_{y_{i'}^+}^{k+t}) \right\} \Delta t, \quad i' \in \mathcal{M}_i^k, \quad (8c)$$

$$o_{i,j}^{k+t} = \begin{cases} 1, & \exists i' \in \mathcal{M}_i^k, y_{i'}^{k+t} \in [j\Delta x, (j+1)\Delta x), u_{i',j}^{k+t} \neq 0 \text{ and } \Gamma_{i',j}^{k+t}, \\ 0, & \forall i' \in \mathcal{M}_i^k, y_{i'}^{k+t} \notin [j\Delta x, (j+1)\Delta x) \text{ or } u_{i',j}^{k+t} = 0 \text{ or } \neg \Gamma_{i',j}^{k+t}, \end{cases} \quad (8d)$$

$$V_i(\boldsymbol{\xi}_i^k, \boldsymbol{\mu}_i^k) \leq \eta_i(\boldsymbol{\xi}_i^k, \lambda_i), \quad (8e)$$

$$\boldsymbol{\rho}_i^{k+0} = \boldsymbol{\rho}^k, \quad \boldsymbol{\rho}_i^{k+t} \in \mathcal{D}, \quad \boldsymbol{\rho}_i^{k+N} \in \mathcal{D}_{i,T}, \quad \max(\mathbf{u}_i^{k+t}) \in U, \quad (8f)$$

$$t \in \{0, 1, \dots, N-1\}, \quad j \in \mathcal{J}, \quad (8g)$$

where $\boldsymbol{\mu}_i^{k*}$ represents the optimal cost control sequence at time k , while $\boldsymbol{\xi}_i^{k*}$ denotes the corresponding prediction state sequence. $\mathcal{M}_i^k \in \mathcal{I}^k$ represents the set of CAVs for which control sequences have already been computed when solving subsystem i at time step k . Since the CAVs execute an agent-by-agent sequential decision-making approach, \mathcal{M}_i^k remains unchanged within the prediction horizon. The position update of CAV $i' \in \mathcal{M}_i^k$ follows the constraint (8c). And CAV $i'' \in \mathcal{I}^k - \mathcal{M}_i^k$ that have not yet obtained their control sequences will temporarily follow the same car-following model as HDVs. $\mathbf{O}_i^{k+t} = [o_{i,0}^{k+t}, o_{i,1}^{k+t}, \dots, o_{i,J}^{k+t}]^T$ indicates whether each cell j contains any controlled CAV. The initial condition is $\boldsymbol{\rho}_i^{k+0} = \boldsymbol{\rho}_i^k$, and the terminal constraint is $\boldsymbol{\rho}_i^{k+N} \in \mathcal{D}_{i,T}$, where $\mathcal{D}_{i,T} \in \mathbb{R}^{J+1}$ is the terminal constraint set for CAV i , and its solution method is detailed in [13]. The sets of states and actions contain certain equilibrium points $(\boldsymbol{\rho}_i^e, \mathbf{u}_i^e)$. This paper assumes that the optimal cost equilibrium point is the origin. The function $\eta_i(\boldsymbol{\xi}_i^k, \lambda_i)$ in constraint (8e) is the contraction function that needs to be designed. The stability objective $V_i(\boldsymbol{\xi}_i^k, \boldsymbol{\mu}_i^k)$ is a classical MPC tracking cost function, designed to ensure that the system gradually converges to the desired state without divergence,

$$V_i(\boldsymbol{\xi}_i^k, \boldsymbol{\mu}_i^k) = \sum_{t=0}^{N-1} L_s(\boldsymbol{\rho}_i^{k+t}, \mathbf{u}_i^{k+t}) + E(\boldsymbol{\rho}_i^{k+N}), \quad (9)$$

$$L_s(\boldsymbol{\rho}_i^{k+t}, \mathbf{u}_i^{k+t}) = \boldsymbol{\rho}_i^{k+tT} \mathbf{Q}_i \boldsymbol{\rho}_i^{k+t} + \mathbf{u}_i^{k+tT} \mathbf{R}_i \mathbf{u}_i^{k+t}, \quad (10)$$

$$E(\boldsymbol{\rho}_i^{k+N}) = \boldsymbol{\rho}_i^{k+N^T} \mathbf{H}_i \boldsymbol{\rho}_i^{k+N}, \quad (11)$$

where the matrices $\mathbf{H}_i \in \mathbb{R}^{(J+1) \times (J+1)}$, $\mathbf{Q}_i \in \mathbb{R}^{(J+1) \times (J+1)}$, and $\mathbf{R}_i \in \mathbb{R}^{(J+1) \times (J+1)}$ are all positive definite and symmetric. \mathbf{Q}_i and \mathbf{R}_i are the given state and control weighting matrices,

respectively. The term $\mathbf{u}_i^{k+tT} \mathbf{R}_i \mathbf{u}_i^{k+t}$ is used to penalize abrupt changes in control actions, thereby promoting smoother control behavior. \mathbf{H}_i is the terminal state weighting matrix, which satisfies the Lyapunov equation [30],

$$\mathbf{Z}_i^T \mathbf{H}_i \mathbf{Z}_i - \mathbf{H}_i = -(\mathbf{Q}_i^* + \Delta \mathbf{Q}_i), \quad \mathbf{Q}_i^* = \mathbf{Q}_i + \mathbf{K}_i^T \mathbf{R}_i \mathbf{K}_i, \quad (12)$$

$\Delta \mathbf{Q}_i \in \mathbb{R}^{(J+1) \times (J+1)}$ is a positive definite matrix, $\mathbf{Z}_i \in \mathbb{R}^{(J+1) \times (J+1)}$ and $\mathbf{K}_i \in \mathbb{R}^{(J+1) \times (J+1)}$ are defined as detailed in Section 3.3.

To construct the contraction function $\eta_i(\xi_i^k, \lambda_i)$, we define the optimization problem for the stability function as,

$$\mu_i^{k,v} = \arg \min_{\mu_i^k} V_i(\xi_i^k, \mu_i^k), \quad (13a)$$

$$\text{s.t. } \rho_i^{k+t+1} = \rho_i^{k+t} + \mathbf{A}_i^{k+t} \mathbf{O}_i^{k+t} + \mathbf{B}_i^{k+t} + \mathbf{C}_{\mathbf{u},i}^{k+t}, \quad (13b)$$

$$y_{i'}^{k+t+1} = y_{i'}^{k+t} + \min \left\{ \max(\mathbf{u}_{i'}^{k+t}), v(\rho_{y_{i'}+}^{k+t}) \right\} \Delta t, \quad i' \in \mathcal{M}_i^k, \quad (13c)$$

$$o_{i,j}^{k+t} = \begin{cases} 1, & \exists i' \in \mathcal{M}_i^k, y_{i'}^{k+t} \in [j\Delta x, (j+1)\Delta x), u_{i',j}^{k+t} \neq 0 \text{ and } \Gamma_{i',j}^{k+t}, \\ 0, & \forall i' \in \mathcal{M}_i^k, y_{i'}^{k+t} \notin [j\Delta x, (j+1)\Delta x) \text{ or } u_{i',j}^{k+t} = 0 \text{ or } \neg \Gamma_{i',j}^{k+t}, \end{cases} \quad (13d)$$

$$\rho_i^{k+0} = \rho^k, \quad \rho_i^{k+t} \in \mathcal{D}, \quad \rho_i^{k+N} \in \mathcal{D}_{i,T}, \quad \max(\mathbf{u}_i^{k+t}) \in U, \quad (13e)$$

$$t \in \{0, 1, \dots, N-1\}, \quad j \in \mathcal{J}, \quad (13f)$$

where $\mu_i^{k,v}$ represents the optimal stability solution at time k . Based on $\mu_i^{k,v}$, the optimal control sequence μ_i^{k-1*} and the corresponding predicted state sequence ξ_i^{k-1*} obtained at time step $k-1$ from the control problem in Eq. (8), we define $\eta_i(\xi_i^k, \lambda_i)$ as

$$\eta_i(\xi_i^k, \lambda_i) = V_i(\xi_i^{k,v}, \mu_i^{k,v}) + \lambda_i \left[V_i(\xi_i^{k-1*}, \mu_i^{k-1*}) - V_i(\xi_i^{k,v}, \mu_i^{k,v}) \right], \quad (14)$$

and $\lambda_i \geq 0$. $\xi_i^{k,v}$ represents the predicted state sequence corresponding to the predictive sequence $\mu_i^{k,v}$.

At each sampling time k , CAV $i \in \mathcal{I}^k$ first minimizes the stability objective function to construct the contraction constraint, and then explores the optimal cost control sequence. If the control problem in Eq. (8) for subsystem i is feasible, the first control input $\mathbf{u}_i^{k*} = \mathbf{u}_i^{k+0*}$ of the final solution μ_i^{k*} is defined as the distributed coupled model predictive control law, $\mathbf{u}_i^k = \mathbf{u}_i^{k*}$. The closed-loop system corresponding to CAV i is,

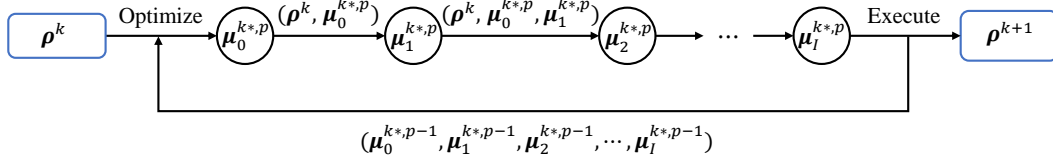
$$\rho_i^{k+1} = \rho_i^k + \mathbf{A}_i^k \mathbf{O}_i^k + \mathbf{B}_i^k + \mathbf{C}_{\mathbf{u},i}^k = \mathbf{g}_i(\rho_i^k, \mathbf{u}_i^k, \mathbf{e}_i^k). \quad (15)$$

Both \mathbf{O}_i^k and $\mathbf{C}_{\mathbf{u},i}^k$ include the position of CAV i and the travel information of all other CAVs. For convenience, we denote this additional information by \mathbf{e}_i^k .

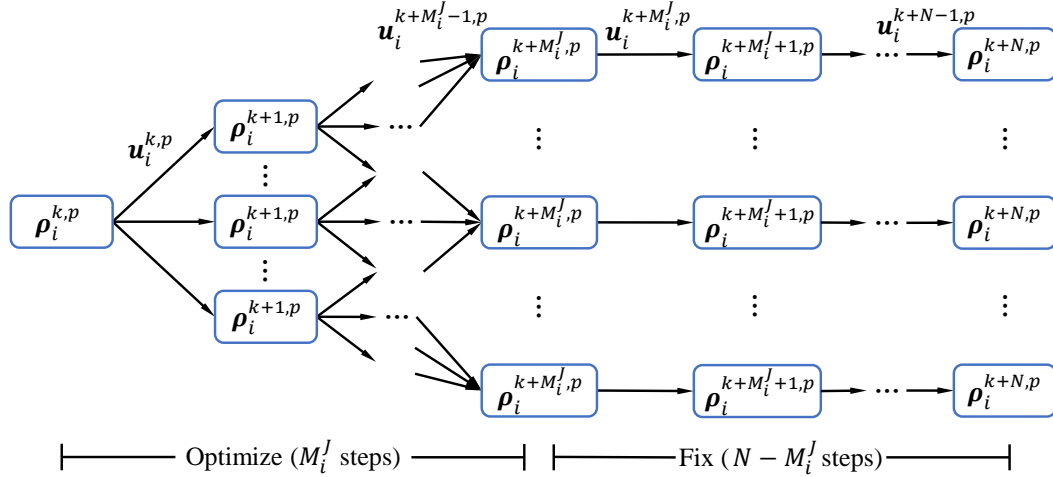
3.1.2 Sequential Optimization with Truncated Rollout

In multiagent systems, although the control objective is global, the degree of cooperation among CAVs significantly affects overall system performance. To address the limitations

of conventional DMPC in handling local optimality, we propose an agent-by-agent iterative optimization approach that enhances coordination among CAVs through real-time policy sharing. As illustrated in Fig. 2(a), at each time step k , the CAVs within the set $\mathcal{I}^k = \{0, 1, \dots, I\}$ sequentially compute their control sequences according to a predetermined order. Iterative refinement is performed after all CAVs complete one round of policy computation to progressively converge towards the optimal control solution. In this section, we assume CAVs execute their optimization in descending index order (i.e., from highest to lowest index). Specifically, during the p -th iteration, each CAV $i \in \mathcal{I}(k)$ receives the latest control sequences $\mu_{0:i-1}^{k*,p}$ from CAV 0 to $i-1$, and the historical control strategies $\mu_{i+1:I}^{k*,p-1}$ from CAV $i+1$ to I . Leveraging the density state transition equation to predict future traffic states, CAV i then solves the optimization problem in Eq. (8) to obtain its optimal control strategy $\mu_i^{k*,p}$. Subsequently, CAV i propagates this updated policy to its succeeding CAVs. This process establishes a sequential cooperative decision chain, ensuring real-time responsiveness and collaborative effectiveness.



(a) Agent-by-agent optimality



(b) Truncated rollout strategy in each iteration

Figure 2: The framework of multiagent truncated rollout approach.

To enhance optimization performance while improving computational efficiency, we propose a truncated rollout optimization strategy (see Fig. 2(b)), which reduces the dimensionality of the optimization variables by truncating the prediction horizon during each iteration [3]. At time step k , the CAVs first execute an N -step prediction to obtain an initial feasible solution $\mu_i^{k*,0} = [\mathbf{u}_i^{k+0*,0}, \mathbf{u}_i^{k+1*,0}, \dots, \mathbf{u}_i^{k+N-1*,0}]$, ensuring the system can make reasonable adjustments in the early stages. During the iteration $p \geq 1$, the prevailing control sequence $\mu_i^{k*,p-1}$ of CAV i is divided into two parts: the first M_i^J steps (where $M_i^J \leq N$)

for optimization, denoted as $\boldsymbol{\mu}_{i,f}^{k*,p-1}$; and the remaining $N - M_i^J$ steps for fixing, denoted as $\boldsymbol{\mu}_{i,r}^{k*,p-1}$,

$$\begin{aligned}\boldsymbol{\mu}_{i,f}^{k*,p-1} &= \left[\mathbf{u}_i^{k+0*,p-1}, \mathbf{u}_i^{k+1*,p-1}, \dots, \mathbf{u}_i^{k+M_i^J-1*,p-1} \right], \\ \boldsymbol{\mu}_{i,r}^{k*,p-1} &= \left[\mathbf{u}_i^{k+M_i^J*,p-1}, \mathbf{u}_i^{k+M_i^J+1*,p-1}, \dots, \mathbf{u}_i^{k+N-1*,p-1} \right].\end{aligned}$$

The controller of CAV i optimizes the first M_i^J control steps based on the current environmental state and $\boldsymbol{\mu}_{i,r}^{k*,p-1}$, while $\boldsymbol{\mu}_{i,r}^{k*,p-1}$ remains unchanged throughout this process. This maintains the control sequence length at N and reduces computational complexity. The value of M_i^J depends on the current system objective function $J_i(\boldsymbol{\xi}_i^{k*,p-1}, \boldsymbol{\mu}_i^{k*,p-1})$,

$$M_i^J = M_{\min} + (N - M_{\min}) \frac{\max \left\{ J_i^{k,LB}, \min \left\{ J_i(\boldsymbol{\xi}_i^{k*,p-1}, \boldsymbol{\mu}_i^{k*,p-1}), J_i^{k,UB} \right\} \right\} - J_i^{k,LB}}{J_i^{k,UB} - J_i^{k,LB}}, \quad (16)$$

where M_{\min} represents the minimum truncation horizon, $J_i^{k,UB}$ and $J_i^{k,LB}$ denote the upper and lower bounds of $J_i(\boldsymbol{\xi}_i^k, \boldsymbol{\mu}_i^k)$, respectively. When the current objective value approaches $J_i^{k,UB}$, it reveals a significant suboptimality gap between the incumbent cost control policy $\boldsymbol{\mu}_i^{k*,p-1}$ and the theoretical Pareto-optimal solution. In this case, increasing the truncation length M_i^J enhances the global search capability of the optimization problem. Conversely, proximity of $J_i(\boldsymbol{\xi}_i^{k*}, \boldsymbol{\mu}_i^{k*})$ to its lower bound $J_i^{k,LB}$ implies that the current policy $\boldsymbol{\mu}_i^{k*,p-1}$ resides within a neighborhood of the local optimum, where the benefit of extended-horizon optimization diminishes. In this situation, adaptively decreasing M_i^J can reduce the computational cost while further approximating the globally optimal solution. The stability function $V_i(\boldsymbol{\xi}_i^k, \boldsymbol{\mu}_i^k)$ is solved iteratively using the same truncation strategy, and

$$M_i^V = M_{\min} + (N - M_{\min}) \frac{\max \left\{ V_i^{k,LB}, \min \left\{ V_i(\boldsymbol{\xi}_i^{k,v,p-1}, \boldsymbol{\mu}_i^{k,v,p-1}), V_i^{k,UB} \right\} \right\} - V_i^{k,LB}}{V_i^{k,UB} - V_i^{k,LB}}. \quad (17)$$

Based on the agent-by-agent optimization property, the state prediction of the last CAV I in Eq. (8b) incorporates the control information propagated from all CAVs in the current iteration. Consequently, the optimization process terminates when the change in the objective value of CAV I between two consecutive iterations falls below a predefined threshold ϵ ,

$$\left| J_I(\boldsymbol{\xi}_I^{k*,p}, \boldsymbol{\mu}_I^{k*,p}) - J_I(\boldsymbol{\xi}_I^{k*,p-1}, \boldsymbol{\mu}_I^{k*,p-1}) \right| \leq \epsilon.$$

3.2 Cost Improvement Properties

In this section, the performance of cost improvement in the multiagent truncated rollout is analyzed through the following propositions.

Proposition 1. *The agent-by-agent sequential decision-making approach, which couples the control actions of other CAVs, is no worse than the parallel decision-making approach.*

Proof. Assume that at any time k , the decisions made by all CAVs in the p -th iteration under the parallel decision-making method are $\mu_0'^{k*,p}, \mu_1'^{k*,p}, \dots, \mu_I'^{k*,p}$, while those made by the agent-by-agent sequential decision-making method are $\mu_0^{k*,p}, \mu_1^{k*,p}, \dots, \mu_I^{k*,p}$. All actions in the control sequences $\mu_i'^{k*,p}$ and $\mu_i^{k*,p}$ of any CAV $i \in \mathcal{I}^k$ are derived from the same control action set U . The corresponding system objective values are $J(\xi'^{k*,p}, \mu_0'^{k*,p}, \mu_1'^{k*,p}, \dots, \mu_I'^{k*,p})$ and $J(\xi^{k*,p}, \mu_0^{k*,p}, \mu_1^{k*,p}, \dots, \mu_I^{k*,p})$. Also, we assume that both methods are based on the optimal solution $\mu_0^{k*,p-1}, \mu_1^{k*,p-1}, \dots, \mu_I^{k*,p-1}$ found in the $(p-1)$ -th iteration.

According to the optimization principles of both methods, the cost improvement for the first CAV relies on the results of the previous iteration,

$$\mu_0^{k*,p} = \mu_0'^{k*,p} = \arg \min_{\mu_0^k} J(\xi_0^k, \mu_0^k, \mu_1^{k*,p-1}, \dots, \mu_I^{k*,p-1}).$$

Thus, the system objective values satisfy,

$$J(\xi_0^k, \mu_0'^{k*,p}, \mu_1^{k*,p-1}, \dots, \mu_I^{k*,p-1}) = J(\xi_0^k, \mu_0^{k*,p}, \mu_1^{k*,p-1}, \dots, \mu_I^{k*,p-1}).$$

For the optimization of strategies for subsequent CAVs, during parallel decision-making, they still execute the control sequence obtained from the $(p-1)$ -th iteration. In contrast, within the sequential decision-making approach, the latest policies of the preceding vehicles in the current iteration is used to replace the results from the previous iteration. This means that during agent-by-agent decision-making, CAVs not only consider the environmental state but also coordinate in real time with the actions of preceding CAVs, ensuring a more optimal overall system objective [6]. As an example, for the second CAV, the sequential method optimizes by considering the latest strategy $\mu_0^{k*,p}$ of the first CAV, whereas the parallel method only uses the $\mu_0^{k*,p-1}$,

$$\begin{aligned} \min_{\mu_1^k} J(\xi_1^k, \mu_0^{k*,p-1}, \mu_1^k, \mu_2^{k*,p-1}, \dots, \mu_I^{k*,p-1}) &= J(\xi_1^k, \mu_0^{k*,p-1}, \mu_1'^{k*,p}, \mu_2^{k*,p-1}, \dots, \mu_I^{k*,p-1}) \\ &\geq J(\xi_1^k, \mu_0'^{k*,p}, \mu_1'^{k*,p}, \mu_2^{k*,p-1}, \dots, \mu_I^{k*,p-1}) \\ &\geq \min_{\mu_1^k} J(\xi_1^k, \mu_0^{k*,p}, \mu_1^k, \mu_2^{k*,p-1}, \dots, \mu_I^{k*,p-1}) \\ &= J(\xi_1^k, \mu_0^{k*,p}, \mu_1^{k*,p}, \mu_2^{k*,p-1}, \dots, \mu_I^{k*,p-1}). \end{aligned}$$

Therefore, extending this reasoning to the entire system, we can obtain,

$$\begin{aligned} \min_{\mu_I^k} J(\xi_I^k, \mu_0^{k*,p-1}, \mu_1^{k*,p-1}, \dots, \mu_{I-1}^{k*,p-1}, \mu_I^k) &= J(\xi_I^k, \mu_0^{k*,p-1}, \mu_1^{k*,p-1}, \dots, \mu_{I-1}^{k*,p-1}, \mu_I'^{k*,p}) \\ &\geq J(\xi_I'^{k*,p}, \mu_0'^{k*,p}, \mu_1'^{k*,p}, \dots, \mu_{I-1}'^{k*,p}, \mu_I'^{k*,p}) \\ &\geq \min_{\mu_I^k} J(\xi_I^k, \mu_0^{k*,p}, \mu_1^{k*,p}, \dots, \mu_{I-1}^{k*,p}, \mu_I^k) \\ &= J(\xi_I^{k*,p}, \mu_0^{k*,p}, \mu_1^{k*,p}, \dots, \mu_{I-1}^{k*,p}, \mu_I^{k*,p}), \end{aligned}$$

which shows that the system performance resulting from sequential decision-making will not be worse than that from parallel decision-making. \square

Proposition 2. *The truncated rollout optimization method can significantly enhance the asymptotic performance of the control strategy and ensure a strict monotonic decrease in the system objective function.*

Proof. Assume that at any time step k , the initial objective function of CAV i is $J_i(\boldsymbol{\xi}_i^{k*,0}, \boldsymbol{\mu}_i^{k*,0})$. With the goal of minimizing $J_i(\boldsymbol{\xi}_i^k, \boldsymbol{\mu}_i^k)$, the first M_i^J steps of the control sequence are optimized in the action set U through truncated rollout approach,

$$\boldsymbol{\mu}_{i,f}^{k*,1} = \arg \min_{\boldsymbol{\mu}_{i,f}^k} J_i \left(\boldsymbol{\xi}_i^k, \boldsymbol{\mu}_{i,f}^k, \boldsymbol{\mu}_{i,r}^{k*,0} \right).$$

The later part of the control sequence $\boldsymbol{\mu}_{i,r}^{k*,0}$ remains unchanged, and the new optimized control sequence is formed,

$$\boldsymbol{\mu}_i^{k*,1} = \left[\boldsymbol{\mu}_{i,f}^{k*,1}, \boldsymbol{\mu}_{i,r}^{k*,0} \right].$$

This process ensures that, at any prediction step $k+t$, the density $\boldsymbol{\rho}_i^{k+t,1} \in \mathcal{D}$, where $t \in \{0, 1, \dots, N\}$. The $\max(\mathbf{u}_i^{k+t,1}) \in U$ satisfies the sequential improvement assumption of the rollout method [5], guaranteeing monotonic improvement of the system objective,

$$J_i \left(\boldsymbol{\xi}_i^{k*,0}, \boldsymbol{\mu}_i^{k*,0} \right) \geq J_i \left(\boldsymbol{\xi}_i^{k*,1}, \boldsymbol{\mu}_i^{k*,1} \right).$$

As the iterations progress, the control sequence of CAV i gradually approaches an approximate optimal solution,

$$J_i \left(\boldsymbol{\xi}_i^{k*,0}, \boldsymbol{\mu}_i^{k*,0} \right) \geq J_i \left(\boldsymbol{\xi}_i^{k*,1}, \boldsymbol{\mu}_i^{k*,1} \right) \geq \dots \geq J_i \left(\boldsymbol{\xi}_i^{k*,p}, \boldsymbol{\mu}_i^{k*,p} \right),$$

i.e., the truncated rollout strategy can effectively improve the control sequence through iterations, achieving superior control performance. \square

3.3 Stability Analysis

In this section, we will prove the stability of the established nonlinear system in Eq. (15). It should be noted that, although the truncated rollout optimizes only the first M steps of the iteration, the constraints of the optimization problem ensure that the complete control sequence, consisting of the optimized and fixed parts, does not affect the stability of the system. We provide several fundamental definitions and assumptions [28],

Definition 1. *Given a discrete-time system $\boldsymbol{\rho}_i^{k+1} = \mathbf{g}_i(\boldsymbol{\rho}_i^k, \mathbf{u}_i^k, \mathbf{e}_i^k)$, a set $\mathcal{D} \subseteq \mathbb{R}^{J+1}$ is called an invariant set if for any state $\boldsymbol{\rho}_i^k \in \mathcal{D}$ and all admissible control inputs $\max(\mathbf{u}_i^k) \in U$, the subsequent state satisfies $\boldsymbol{\rho}_i^{k+1} \in \mathcal{D}$.*

Definition 2. *For the system in Definition 1 with invariant set \mathcal{D} , the system is input-to-state stability (ISS) within \mathcal{D} if for any initial condition $\boldsymbol{\rho}_i^k \in \mathcal{D}$, there exists a KL-class function $\beta : \mathbb{R}_{\geq 0} \times \mathbb{N} \rightarrow \mathbb{R}_{\geq 0}$ such that the state trajectory satisfies [30],*

$$\|\boldsymbol{\rho}_i^{k+t}\|_{\mathcal{D}} \leq \beta(\|\boldsymbol{\rho}_i^k\|, t), \forall t \in \{0, 1, 2, \dots, N-1\},$$

where $\boldsymbol{\rho}_i^{k+t}$ denotes the state response at time $k+t$ with initial condition $\boldsymbol{\rho}_i^k$, $\|\cdot\|$ is the induced norm of the set \mathcal{D} .

Lemma 1. For the system $\rho_i^{k+1} = \mathbf{g}_i(\rho_i^k, \mathbf{u}_i^k, \mathbf{e}_i^k)$ and invariant set $\mathcal{D} \subseteq \mathbb{R}^{J+1}$, if there exists a function $V_i(\xi_i^k, \mu_i^k) : \mathbb{R}^{J+1} \times \mathbb{R}^{J+1} \rightarrow \mathbb{R}_{\geq 0}$ such that for all $\rho_i^k \in \mathcal{D}$ the following conditions hold,

$$\begin{aligned} \alpha_1(\|\rho_i^k\|) &\leq V_i(\xi_i^k, \mu_i^k) \leq \alpha_2(\|\rho_i^k\|), \\ V_i(\xi_i^{k+1}, \mu_i^{k+1}) - V_i(\xi_i^k, \mu_i^k) &\leq -\alpha_3(\|\rho_i^k\|), \end{aligned}$$

where $\alpha_1(\cdot)$, $\alpha_2(\cdot)$, and $\alpha_3(\cdot)$ are K_∞ class functions, then $V_i(\xi_i^k, \mu_i^k)$ is referred to as an ISS-Lyapunov function for the system, and the system is ISS within the invariant set \mathcal{D} .

Definition 3. Consider the closed-loop system $\rho_i^{k+1} = \mathbf{g}_i(\rho_i^k, \mathbf{u}_i^k, \mathbf{e}_i^k)$, and let $\mathcal{D} \subseteq \mathbb{R}^{J+1}$ be an invariant set of the system. A state $\rho_i^k \in \mathcal{D}$ is called a feasible initial state if there exists a feasible predictive control sequence $\mu_i^k = [\mathbf{u}_i^k, \mathbf{u}_i^{k+1}, \dots, \mathbf{u}_i^{k+N-1}]$ such that the closed-loop trajectory satisfies $\rho_i^{k+t} \in \mathcal{D}$ for all $t \in \{0, 1, \dots, N-1\}$. The set of all such feasible initial states is denoted by \mathcal{D}_N , which satisfies $\mathcal{D}_{i,T} \subseteq \mathcal{D}_N \subseteq \mathcal{D}$, where $\mathcal{D}_{i,T}$ denotes the terminal constraint set.

Assumption 1. The environmental state ρ^k is globally observable, and all subsystems share identical environmental states,

$$\rho_0^k = \rho_1^k = \dots = \rho_I^k = \rho^k.$$

Assumption 2. During the prediction horizon $[k, k+N]$, the number of CAVs in the system remains constant, that is, no new CAVs are allowed to enter. For any CAV that exits the system at time step $k+t$ within the prediction horizon, its control inputs are assumed to be zero for the remaining time steps $[k+t+1, k+N]$.

Assumption 3. There exists a local linear feedback control law $\mathbf{u}_i^k = \mathbf{K}_i \rho_i^k$, where $\mathbf{K}_i \in \mathbb{R}^{(J+1) \times (J+1)}$, such that $\max(\mathbf{u}_i^k) \in U$ holds for all $\rho_i^k \in \mathcal{D}_{i,T}$. The design of this control law is based on the linearization of the system in Eq. (15) around the origin (an asymptotically stable equilibrium point), given by,

$$\rho_i^{k+1} = \psi_i \rho_i^k + \delta_i \mathbf{u}_i^k, \quad (18)$$

where $\psi_i = \frac{\partial \mathbf{g}_i}{\partial \rho_i} \big|_{\rho_i=0}$ and $\delta_i = \frac{\partial \mathbf{g}_i}{\partial \mathbf{u}_i} \big|_{\mathbf{u}_i=0}$. The resulting closed-loop matrix $\mathbf{Z}_i = \psi_i + \delta_i \mathbf{K}_i$ is Schur stable, $\mathbf{Z}_i \in \mathbb{R}^{(J+1) \times (J+1)}$ [30].

Lemma 2. If Assumptions 1 and 3 hold, then the terminal constraint set $\mathcal{D}_{i,T}$ is an invariant set for the closed-loop system in Eq. (15), and for any $\rho_i^k \in \mathcal{D}_{i,T}$, the following inequality always holds,

$$E(\psi_i \rho_i^k + \delta_i \mathbf{u}_i^k) - E(\rho_i^k) \leq -L_s(\rho_i^k, \mathbf{K}_i \rho_i^k).$$

Proof. According to Assumption 3, for any $\rho_i^k \in \mathcal{D}_{i,T}$, the local control law $\mathbf{u}_i^k = \mathbf{K}_i \rho_i^k$ is feasible, and the state evolution follows $\rho_i^{k+1} = \mathbf{Z}_i \rho_i^k$, where $\mathbf{Z}_i = \psi_i + \delta_i \mathbf{K}_i$. Furthermore, $E(\rho_i^k)^{\frac{1}{2}} \leq \varepsilon$ within $\mathcal{D}_{i,T}$. Taking the difference of the function $E(\rho_i^{k+1})$, and using Eq. (12), we have,

$$E(\rho_i^{k+1}) - E(\rho_i^k) = E(\psi_i \rho_i^k + \delta_i \mathbf{u}_i^k) - E(\rho_i^k)$$

$$\begin{aligned}
&= E(\psi_i \rho_i^k + \delta_i \mathbf{K}_i \rho_i^k) - E(\rho_i^k) \\
&= E(\mathbf{Z}_i \rho_i^k) - E(\rho_i^k) \\
&= \rho_i^{kT} \mathbf{Z}_i^T \mathbf{H}_i \mathbf{Z}_i \rho_i^k - \rho_i^{kT} \mathbf{H}_i \rho_i^k \\
&= \rho_i^{kT} (\mathbf{Z}_i^T \mathbf{H}_i \mathbf{Z}_i - \mathbf{H}_i) \rho_i^k \\
&= \rho_i^{kT} [-(\mathbf{Q}_i^* + \Delta \mathbf{Q}_i)] \rho_i^k \\
&= \rho_i^{kT} [-(\mathbf{Q}_i + \mathbf{K}_i^T \mathbf{R}_i \mathbf{K}_i + \Delta \mathbf{Q}_i)] \rho_i^k \\
&= -\rho_i^{kT} \mathbf{Q}_i \rho_i^k - \rho_i^{kT} \mathbf{K}_i^T \mathbf{R}_i \mathbf{K}_i \rho_i^k - \rho_i^{kT} \Delta \mathbf{Q}_i \rho_i^k \\
&= -L_s(\rho_i^k, \mathbf{K}_i \rho_i^k) - \rho_i^{kT} \Delta \mathbf{Q}_i \rho_i^k \\
&\leq -L_s(\rho_i^k, \mathbf{K}_i \rho_i^k).
\end{aligned}$$

Since $L_s(\rho_i^k, \mathbf{K}_i \rho_i^k)$ is a positive definite function, it follows that $E(\rho_i^{k+1}) - E(\rho_i^k) \leq 0$, which implies $E(\rho_i^{k+1})^{\frac{1}{2}} \leq E(\rho_i^k)^{\frac{1}{2}} \leq \varepsilon$. According to Definition 1, this indicates that the set $\mathcal{D}_{i,T}$ is an invariant set for the closed-loop system in Eq. (15). \square

Next, we demonstrate the recursive feasibility of the optimal control problem in Eq. (8) and the stability of the closed-loop system in Eq. (15).

Theorem 1. *If Assumptions 1 and 3 hold, then for any given $\lambda_i \geq 0$, the optimal control problem in Eq. (8) is recursively feasible within the feasible initial state set \mathcal{D}_N , and \mathcal{D}_N is an invariant set for the closed-loop system in Eq. (15).*

Proof. First, based on the state of subsystem i at time step $k-1$, denoted as $\rho_i^{k-1} \in \mathcal{D}_N$, and the corresponding optimal control sequence of the optimization problem in Eq. (8) $\mu_i^{k-1*} = [\mathbf{u}_i^{k-1+0*}, \mathbf{u}_i^{k-1+1*}, \dots, \mathbf{u}_i^{k-1+N-1*}]$, as well as the associated optimal predicted state sequence $\xi_i^{k-1*} = [\rho_i^{k-1+1*}, \rho_i^{k-1+2*}, \dots, \rho_i^{k-1+N*}]$, we construct a control sequence at time k ,

$$\hat{\mu}_i^k = [\mathbf{u}_i^{k-1+1*}, \mathbf{u}_i^{k-1+2*}, \dots, \mathbf{u}_i^{k-1+N-1*}, \mathbf{K}_i \rho_i^{k-1+N*}].$$

Since the terminal state ρ_i^{k-1+N*} belongs to the terminal set $\mathcal{D}_{i,T}$, and the local control law $\mathbf{u}_i^{k-1+N*} = \mathbf{K}_i \rho_i^{k-1+N*}$ ensures that $\max(\mathbf{u}_i^{k-1+N*}) \in U$, the constructed control sequence $\hat{\mu}_i^k$ satisfies the control constraint (8f). The corresponding predicted state sequence is,

$$\hat{\xi}_i^k = [\rho_i^{k-1+2*}, \rho_i^{k-1+3*}, \dots, \rho_i^{k-1+N*}, \hat{\rho}_i^{k+N}],$$

where $\hat{\rho}_i^{k+N} = \psi_i \rho_i^{k-1+N*} + \delta_i \mathbf{K}_i \rho_i^{k-1+N*}$. According to Lemma 2, $\hat{\rho}_i^{k+N} \in \mathcal{D}_{i,T}$, implying that $\hat{\xi}_i^k$ satisfies the state constraints, and $E(\hat{\rho}_i^{k+N}) - E(\rho_i^{k-1+N*}) \leq -L_s(\rho_i^{k-1+N*}, \mathbf{K}_i \rho_i^{k-1+N*})$. Therefore, the control sequence $\hat{\mu}_i^k$ satisfies all the constraints of the stability optimization problem in Eq. (13), ensuring the feasibility of the problem at time k .

Assume that the optimal solution of the problem in Eq. (13) at time k is $\mu_i^{k,v}$, and $V_i(\xi_i^{k,v}, \mu_i^{k,v}) \leq V_i(\xi_i^k, \hat{\mu}_i^k)$. By comparing the optimal cost values at consecutive time steps, we have,

$$V_i(\xi_i^{k,v}, \mu_i^{k,v}) - V_i(\xi_i^{k-1*}, \mu_i^{k-1*})$$

$$\begin{aligned}
&\leq V_i(\hat{\xi}_i^k, \hat{\mu}_i^k) - V_i(\xi_i^{k-1*}, \mu_i^{k-1*}) \\
&= E(\hat{\rho}_i^{k+N}) + \sum_{t=1}^{N-1} L_s(\rho_i^{k-1+t*}, \mathbf{u}_i^{k-1+t*}) + L_s(\rho_i^{k-1+N*}, \mathbf{K}_i \rho_i^{k-1+N*}) \\
&\quad - E(\rho_i^{k-1+N*}) - \sum_{t=0}^{N-1} L_s(\rho_i^{k-1+t*}, \mathbf{u}_i^{k-1+t*}) \\
&= E(\hat{\rho}_i^{k+N}) - E(\rho_i^{k-1+N*}) + L_s(\rho_i^{k-1+N*}, \mathbf{K}_i \rho_i^{k-1+N*}) - L_s(\rho_i^{k-1*}, \mathbf{u}_i^{k-1*}) \\
&\leq -L_s(\rho_i^{k-1+N*}, \mathbf{K}_i \rho_i^{k-1+N*}) + L_s(\rho_i^{k-1+N*}, \mathbf{K}_i \rho_i^{k-1+N*}) - L_s(\rho_i^{k-1*}, \mathbf{u}_i^{k-1*}) \\
&= -L_s(\rho_i^{k-1*}, \mathbf{u}_i^{k-1*}) \\
&\leq 0.
\end{aligned} \tag{19}$$

Hence, in the contraction function $\eta_i(\xi_i^k, \lambda_i)$, we have $V_i(\xi_i^{k-1*}, \mu_i^{k-1*}) - V_i(\xi_i^{k,v}, \mu_i^{k,v}) \geq 0$, and for any $\lambda_i \geq 0$, it holds that $\eta_i(\xi_i^k, \lambda_i) \geq 0$ and $V_i(\xi_i^{k,v}, \mu_i^{k,v}) \leq \eta_i(\xi_i^k, \lambda_i)$. Therefore, $\mu_i^{k,v}$ is a feasible solution to Eq. (8), demonstrating that the problem exhibits recursive feasibility.

Consequently, for any $\rho_i^k \in \mathcal{D}_N$, there exists a feasible solution such that the successor state $\rho_i^{k+1} = \mathbf{g}_i(\rho_i^k, \mathbf{u}_i^k, \mathbf{e}_i^k) \in \mathcal{D}_N$. According to Definitions 1 and 3, the set \mathcal{D}_N is positively invariant under the closed-loop system in Eq. 15. \square

Theorem 2. *If Assumptions 1 and 3 hold and the optimal control problem in Eq. (8) admits a feasible solution at the initial time, then for any $\lambda_i \in [0, 1)$, the closed-loop system in Eq. (15) is ISS within the invariant set \mathcal{D}_N .*

Proof. From the Eq. (9), we have,

$$\alpha_{i,1}(\|\rho_i^k\|) = q \times \|\rho_i^k\|^2 \leq L_s(\rho_i^k, \mathbf{u}_i^k) \leq V_i(\xi_i^k, \mu_i^k),$$

where q denotes the minimum eigenvalue of matrix \mathbf{Q}_i , and $\alpha_{i,1}(\|\rho_i^k\|)$ is a K_∞ class function, which can be regarded as a lower bound of the stability function $V_i(\xi_i^k, \mu_i^k)$ at time step k .

To establish an upper bound for the stability function, we define,

$$\begin{aligned}
L_{s,\max} &= \max \{L_s(\rho_i^k, \mathbf{u}_i^k) \mid \rho_i^k \in \mathcal{D}_N, \max(\mathbf{u}_i^k) \in U\}, \\
E_{\max} &= \max \{E(\rho_i^k) \mid \rho_i^k \in \mathcal{D}_N\}.
\end{aligned}$$

Then it follows that,

$$V_i(\xi_i^k, \mu_i^k) \leq E_{\max} + NL_{s,\max}.$$

Based on this, we construct a function,

$$\alpha_{i,2}(\|\rho_i^k\|) = \theta \times \|\rho_i^k\|^2,$$

with a properly chosen parameter $\theta \geq 0$, such that,

$$\theta \times \|\rho_i^k\|^2 \geq E_{\max} + NL_{s,\max}, \quad \forall \rho_i^k \in \mathcal{D}_N.$$

This ensures that $V_i(\boldsymbol{\xi}_i^k, \boldsymbol{\mu}_i^k) \leq \alpha_{i,2}(\|\boldsymbol{\rho}_i^k\|)$, and $\alpha_{i,2}(\|\boldsymbol{\rho}_i^k\|)$ is a K_∞ class function.

According to the recursive feasibility established in Theorem 1, a feasible solution exists at every time step k . Consider the optimal solutions at two consecutive time steps, $\boldsymbol{\mu}_i^{k-1*}$ and $\boldsymbol{\mu}_i^{k*}$. When $\lambda_i \in [0, 1)$, from the contraction constraint (8e) and the Eq. (19), we obtain,

$$\begin{aligned} V_i(\boldsymbol{\xi}_i^{k*}, \boldsymbol{\mu}_i^{k*}) - V_i(\boldsymbol{\xi}_i^{k-1*}, \boldsymbol{\mu}_i^{k-1*}) &\leq (1 - \lambda_i) \left[V_i(\boldsymbol{\xi}_i^{k,v}, \boldsymbol{\mu}_i^{k,v}) - V_i(\boldsymbol{\xi}_i^{k-1*}, \boldsymbol{\mu}_i^{k-1*}) \right] \\ &\leq (1 - \lambda_i) \left[-L_s(\boldsymbol{\rho}_i^{k-1*}, \mathbf{u}_i^{k-1*}) \right] \\ &\leq (1 - \lambda_i) \left[q \times \|\boldsymbol{\rho}_i^{k-1*}\|^2 \right] \\ &= -(\lambda_i - 1)\alpha_{i,1}(\|\boldsymbol{\rho}_i^{k-1*}\|) \\ &= -\alpha_{i,3}(\|\boldsymbol{\rho}_i^{k-1*}\|), \end{aligned}$$

where $\alpha_{i,3}(\|\boldsymbol{\rho}_i^{k-1*}\|)$ is also a K_∞ class function. Clearly, this implies that,

$$V_i(\boldsymbol{\xi}_i^{k*}, \boldsymbol{\mu}_i^{k*}) \leq V_i(\boldsymbol{\xi}_i^{k-1*}, \boldsymbol{\mu}_i^{k-1*}),$$

i.e., the value function $V_i(\boldsymbol{\xi}_i^k, \boldsymbol{\mu}_i^k)$ is monotonically decreasing along the closed-loop trajectory.

In conclusion, the value function $V_i(\boldsymbol{\xi}_i^k, \boldsymbol{\mu}_i^k)$ satisfies the key conditions of Lemma 1. Therefore, it qualifies as an ISS-Lyapunov function for subsystem i , and subsystem i is ISS within the invariant set \mathcal{D}_N . \square

In the multiagent truncated rollout framework, the optimization problem for each subsystem is solved sequentially while incorporating control inputs from all other CAVs. The terminal subsystem, by aggregating the ISS properties of all constituent subsystems, guarantees the stability of the overall system within the invariant set \mathcal{D}_N .

4 Computational Issues in Rollout Algorithms

In this section, we analyze the computational complexity of the multiagent truncated rollout method and compare it with centralized model predictive control (MPC) and distributed model predictive control (DMPC) approaches (Section 4.1). We also investigate the optimal decision sequence for CAVs (Section 4.2) and derive theoretical error bounds for the objective function (Section 4.3). These analyses establish the foundation for the performance and stability assurances of the proposed control scheme. We finally present the detailed solution algorithms for implementing the proposed strategy in multiagent environments (Section 4.4).

4.1 Time Complexity Analysis

In this subsection, we systematically compare and analyze the computational complexity reduction afforded by this approach in a multiagent system comprising $(I + 1)$ CAVs. We assume that each CAV has a prediction and control horizon of N and that its control action space is discretized into a set containing S discrete control actions at any prediction time $k + t$.

It is known that in centralized MPC, the dynamic behavior of all subsystems is managed by a central controller, which collects system state information and computes the globally optimal control inputs for all CAVs. Although this approach can account for the cooperation of all CAVs and theoretically achieve a global optimum, as the system scale increases, the number of variables and constraints that the central controller must handle grows significantly. In the assumed environment, at each time step, the algorithm is required to predict the control actions of all CAVs over the optimal horizon N . Consequently, the computational complexity grows exponentially with both the number of CAVs and the prediction horizon, and is given by $O(S^{(I+1) \times N})$.

In DMPC, the overall system is decomposed into multiple subsystems, where each subsystem solves its own optimization problem independently. Over the prediction horizon N , the complexity for each CAV is $O(S^N)$, and the total system complexity can be expressed as $O(S^N \times (I + 1))$. However, the individually optimal solutions of CAVs do not necessarily coincide with the system global optimum, and independent solving leads to poor coordination among agents. To address this, CAVs are allowed multiple rounds of communication, iteratively optimizing their control actions after acquiring updated control information from other CAVs. Although the iterative optimization introduces some computational delay, in practice, the number of iterations required for the system to converge to an approximately optimal solution is quite small (e.g., $P = 3$ to 5). Moreover, in large-scale systems, computational complexity that grows linearly with $(I + 1)$ is significantly lower than complexity that grows exponentially. This enables DMPC to often achieve shorter computation times and better scalability than centralized MPC within a limited number of iterations.

Different from traditional DMPC, the proposed multiagent truncated rollout method not only adopts an agent-by-agent approach to convert the coordination of multiple subsystems into sequential interactions, but also employs truncated rollout during the iteration process to reduce the optimization horizon. As shown in Table 1, at each iteration, each CAV i optimizes only the first $M_i^J \leq N$ steps of its control sequence, reducing the computational complexity for a single vehicle to $O(S^{M_i^J})$. Consequently, the overall computational complexity per iteration is reduced to $O(\sum_{i=0}^I S^{M_i^J})$.

Table 1: Comparison of computational complexity.

Approach	Time complexity
Model predictive control	$O(S^{N \times (I+1)})$
Distributed model predictive control	$O(S^N \times (I + 1))$
Multiagent truncated rollout	$O(\sum_{i=0}^I S^{M_i^J})$

4.2 Decision Order Optimization

In the agent-by-agent sequential decision-making framework, the order in which CAVs make decisions directly impacts the quality of the generated strategies. In this section, we propose a dynamic decision-ordering mechanism that reconstructs the decision sequence in multiagent

truncated rollout algorithms by evaluating the potential contribution of each CAV to the overall traffic state at the current time step. This approach aims to improve system-level performance while preserving the cost improvement property of rollout [4].

Specifically, at each time step k , the decision order of the CAVs is determined through the following steps,

(1) For all CAVs $i \in \{0, 1, \dots, I\}$, the optimal objective value $J_i(\xi_i^{k*}, \mu_i^{k*})$ is evaluated in parallel under the assumption that CAV i is the first to optimize, while all other CAVs follow a predefined car-following model. The CAV with the lowest objective value is selected as the first agent to optimize,

$$i_0^* = \arg \min_{i \in \{0, 1, \dots, I\}} J_i(\xi_i^{k*}, \mu_i^{k*}).$$

(2) Fix the control result of CAV i_0^* , i.e., $\mu_{i_0^*}^{k*}$, and for the remaining CAVs, compute in parallel their optimal objective values assuming each is the second decision-maker, while the others continue to follow the car-following model. The one with the lowest cost is selected as the second decision-maker.

(3) Repeat the above procedure until a complete decision sequence $i_0^* \rightarrow i_1^* \rightarrow \dots \rightarrow i_I^*$ is obtained. This also yields an initial joint control input $\mu_{i_0^*:i_I^*}^{k*}$ for all CAVs at time step k .

This dynamic mechanism ensures that CAVs with greater influence on traffic dynamics are prioritized in decision-making, thereby providing more accurate future-state predictions for subsequent vehicles. Although this method requires a total of $(I + 1) + I + \dots + 1 = (I + 1)(I + 2)/2$ objective function evaluations, the computational burden is substantially alleviated through parallel processing, making the runtime comparable to that of agent-by-agent rollout with a fixed decision order.

4.3 Error Bounds for the Objective Function

In Eq. (16) and Eq. (17), the selection of the truncated horizons M_i^J and M_i^V is related to the upper and lower bounds of the corresponding objective functions. According to Lemma 1 and Theorem 2, there exist two K_∞ class functions, $\alpha_{i,1}(\|\rho_i^k\|) = q \times \|\rho_i^k\|^2$ and $\alpha_{i,2}(\|\rho_i^k\|) = \theta \times \|\rho_i^k\|^2$, such that the stability objective function $V_i(\xi_i^k, \mu_i^k)$ satisfies,

$$\alpha_{i,1}(\|\rho_i^k\|) \leq V_i(\xi_i^k, \mu_i^k) \leq \alpha_{i,2}(\|\rho_i^k\|). \quad (20)$$

This implies that the upper and lower bounds of the function $V_i(\xi_i^k, \mu_i^k)$ are determined by $\alpha_{i,1}(\|\rho_i^k\|)$ and $\alpha_{i,2}(\|\rho_i^k\|)$, respectively. Next, we derive similar bounds for the control objective function $J_i(\xi_i^k, \mu_i^k)$.

Proposition 3. *Let $\mu_i^{k,v}$ be the optimal solution of the stability objective function $V_i(\xi_i^k, \mu_i^k)$ at time step k in Eq. (13). When the jam density of each road cell is R , and the set of control actions for CAV $i \in \mathcal{I}^k$ is $U = [u_{\min}, u_{\max}]$, the optimal value μ_i^{k*} of the control objective function $J_i(\xi_i^k, \mu_i^k)$ in Eq. (8) satisfies,*

$$\frac{\Delta x \Delta t}{q} \left[V_i(\xi_i^{k,v}, \mu_i^{k,v}) - N r u_{\max}^2 - (J + 1) h R^2 \right] \leq J_i(\xi_i^{k*}, \mu_i^{k*}) \leq J_i(\xi_i^{k,v}, \mu_i^{k,v}), \quad (21)$$

where q , r , and h are the maximum values in the state weighting matrix \mathbf{Q}_i , control action weighting matrix \mathbf{R}_i , and terminal state weighting matrix \mathbf{H}_i , respectively.

Proof. First, we explain the upper bound of the $J_i(\boldsymbol{\xi}_i^{k*}, \boldsymbol{\mu}_i^{k*})$. From Eq. (19), the optimal solution $\boldsymbol{\mu}_i^{k-1*}$ of the stability objective function at time step $k-1$ satisfies,

$$V_i(\boldsymbol{\xi}_i^{k-1*}, \boldsymbol{\mu}_i^{k-1*}) - V_i(\boldsymbol{\xi}_i^{k,v}, \boldsymbol{\mu}_i^{k,v}) \geq 0.$$

When $\lambda_i \leq 0$, we have,

$$V_i(\boldsymbol{\xi}_i^{k,v}, \boldsymbol{\mu}_i^{k,v}) \leq V_i(\boldsymbol{\xi}_i^{k,v}, \boldsymbol{\mu}_i^{k,v}) + \lambda_i [V_i(\boldsymbol{\xi}_i^{k-1*}, \boldsymbol{\mu}_i^{k-1*}) - V_i(\boldsymbol{\xi}_i^{k,v}, \boldsymbol{\mu}_i^{k,v})].$$

This implies that $\boldsymbol{\mu}_i^{k,v}$ satisfies constraints (8b)-(8e), and it is a feasible solution to the control problem in Eq. (8), but not necessarily the optimal one. Based on the minimization property of the objective function, we can conclude,

$$J_i(\boldsymbol{\xi}_i^{k*}, \boldsymbol{\mu}_i^{k*}) \leq J_i(\boldsymbol{\xi}_i^{k,v}, \boldsymbol{\mu}_i^{k,v}).$$

Next, we prove the lower bound of $J_i(\boldsymbol{\xi}_i^{k*}, \boldsymbol{\mu}_i^{k*})$. From the definition of $V_i(\boldsymbol{\xi}_i^k, \boldsymbol{\mu}_i^k)$ in Eq. (9)-(11), we obtain,

$$\begin{aligned} V_i(\boldsymbol{\xi}_i^k, \boldsymbol{\mu}_i^k) &= \sum_{t=0}^{N-1} \left(\boldsymbol{\rho}_i^{k+tT} \mathbf{Q}_i \boldsymbol{\rho}_i^{k+t} + \mathbf{u}_i^{k+tT} \mathbf{R}_i \mathbf{u}_i^{k+t} \right) + \boldsymbol{\rho}_i^{k+N^T} \mathbf{H}_i \boldsymbol{\rho}_i^{k+N} \\ &\leq \sum_{t=0}^{N-1} \left(q \sum_{j=0}^J \rho_{i,j}^{k+t^2} + r \sum_{j=0}^J u_{i,j}^{k+t^2} \right) + h \sum_{j=0}^J \rho_{i,j}^{k+N^2}. \end{aligned}$$

Since only the action of the cell where CAV i is located is non-zero in \mathbf{u}_i^{k+t} , and $\max(\mathbf{u}_i^{k+t}) \leq u_{\max}$,

$$r \sum_{j=0}^J u_{i,j}^{k+t^2} \leq r u_{\max}^2.$$

Similarly, for each cell j , $\rho_{i,j}^{k+N} \leq R$,

$$h \sum_{j=0}^J \rho_{i,j}^{k+N^2} \leq (J+1)hR^2.$$

Thus,

$$V_i(\boldsymbol{\xi}_i^{k,v}, \boldsymbol{\mu}_i^{k,v}) \leq V_i(\boldsymbol{\xi}_i^k, \boldsymbol{\mu}_i^k) \leq q \sum_{t=0}^{N-1} \sum_{j=0}^J \rho_{i,j}^{k+t^2} + N r u_{\max}^2 + (J+1)hR^2,$$

and then,

$$\sum_{t=0}^{N-1} \sum_{j=0}^J \rho_{i,j}^{k+t^2} \geq \frac{1}{q} \left[V_i(\boldsymbol{\xi}_i^{k,v}, \boldsymbol{\mu}_i^{k,v}) - N r u_{\max}^2 - (J+1)hR^2 \right],$$

where $q > 0$.

Since the vehicle density in each cell j satisfies $\rho_{i,j}^{k+t} < 1$, so $\rho_{i,j}^{k+t} > \rho_{i,j}^{k+t^2}$ and

$$\sum_{t=0}^{N-1} \sum_{j=0}^J \rho_{i,j}^{k+t} > \sum_{t=0}^{N-1} \sum_{j=0}^J \rho_{i,j}^{k+t^2}.$$

Consequently,

$$\begin{aligned} J_i(\xi_i^k, \mu_i^k) &= \sum_{t=0}^{N-1} \sum_{j=0}^J \rho_{i,j}^{k+t} \Delta x \Delta t \\ &\geq J_i(\xi_i^{k*}, \mu_i^{k*}) \\ &> \sum_{t=0}^{N-1} \sum_{j=0}^J \rho_{i,j}^{k+t^2} \Delta x \Delta t \\ &\geq \frac{\Delta x \Delta t}{q} \left[V_i(\xi_i^{k,v}, \mu_i^{k,v}) - Nru_{\max}^2 - (J+1)hR^2 \right]. \end{aligned}$$

□

4.4 Solution Algorithm

Building on the previously introduced CAV decision order optimization method and the objective function bounds evaluation mechanism, this subsection outlines the overall algorithmic framework for achieving efficient coordination among multiple CAVs. We divide the multiagent truncated rollout method into two key components: (1) optimal control sequence solving for individual CAVs, and (2) a sequential iteration scheme for all CAVs.

As described in Section 3.1.1, at each time step $k \in \{1, 2, \dots\}$, the optimal control sequence for CAV $i \in \mathcal{I}^k$ is determined by solving the problem defined in Eq. (8). CAV i first minimizes the stability function $V_i(\xi_i^k, \mu_i^k)$ to generate a candidate control sequence $\mu_i^{k,v,p}$. Subsequently, a contraction constraint $\eta_i(\xi_i^k, \lambda_i)$ is constructed to ensure system stability while optimizing the cost objective function, yielding the optimal control sequence $\mu_i^{k*,p}$. During the iterative process, the optimization horizons M_i^V and M_i^J ($M_i^V \leq N$ and $M_i^J \leq N$) are dynamically adjusted: initialization employs the full horizon N , followed by adaptive truncation of the prediction horizon based on evaluating solution quality using the upper and lower bounds of the objective functions ($J_i^{k,UB}$, $J_i^{k,LB}$ or $V_i^{k,UB}$, $V_i^{k,LB}$). This strategy effectively reduces computational burden without significantly compromising performance.

To coordinate the control decisions of all CAVs within the total optimization horizon $T\Delta t$ while minimizing the cumulative travel time of all vehicles, we propose an iterative scheme as detailed in Algorithm 1. At each time step k , the impact of individual CAVs on traffic efficiency is evaluated under the current state to optimize the decision-making order and generate initial solutions. Then, CAVs sequentially implement iterative improvements to this initial solution according to the fixed optimization order. It is important to note that when the time step $k + N$ exceeds T , both the prediction and control horizons of the controlled CAV are adjusted to $T - k$.

Algorithm 1 Multiagent truncated rollout algorithm.

Input: Total optimization time $T\Delta t$; Termination condition ϵ ; Prediction horizon N ; Objective function $J_i(\xi_i^k, \mu_i^k)$;
Output: Total travel time J_t of vehicles on the road during optimization time $T\Delta t$;

- 1: Initialize $J_t := 0$;
- 2: **for** $k = 0$ to $T - 1$ **do**
- 3: Get traffic state ρ^k and construct the set of the CAVs $\mathcal{I}^k = \{1, 2, \dots, I\}$;
- 4: Set the objective function difference $\Delta := +\infty$;
- 5: $J_t \leftarrow J_t + \sum_{j=0}^J [\rho_j^k \times \Delta t \times \Delta x]$;
- 6: Set the iteration count $p := 0$;
- 7: Conduct parallel evaluation of the $J_i(\xi_i^k, \mu_i^k)$ for all CAVs;
- 8: Generate the decision sequence ℓ^k and initial solution set $\mu_{0:I}^{k*,0}$;
- 9: **while** $\Delta > \epsilon$ **do**
- 10: $p \leftarrow p + 1$;
- 11: **for each** CAV i in ℓ^k **do**
- 12: Calculate the truncated horizon M_i^V and solve stability control problem to obtain $\mu_i^{k,v,p}$;
- 13: Calculate the truncated horizon M_i^J and solve cost control problem to obtain $\mu_i^{k*,p}$;
- 14: **end for**
- 15: $\Delta \leftarrow \left| J_I(\xi_i^{k,p}, \mu_i^{k,p}) - J_I(\xi_i^{k,p-1}, \mu_i^{k,p-1}) \right|$;
- 16: **end while**
- 17: Execute the first control action \mathbf{u}_i^{k*} for all CAV $i \in \mathcal{I}^k$.
- 18: **end for**

5 Numerical Results

In this section, we present numerical experiments to validate the proposed method. We outline the experimental settings (Section 5.1) and evaluate the performance of the multiagent truncated rollout through comparisons with several state-of-the-art baseline algorithms (Section 5.2). To provide further insights, we then apply the method to diverse traffic scenarios and conduct sensitivity analyses (Section 5.3). Finally, we analyze the scalability of the multiagent truncated rollout approach on large-scale transportation systems (Section 5.4).

5.1 Experimental Settings

We select a real-world bottleneck section of the Hujin Highway in Shanghai, China, as the case study. The simulation environment is constructed using the simulation of urban mobility (SUMO) platform [25]. As shown in Fig. 3, a 3000 m segment with a lane reduction from three to two lanes is modeled, where a 2100 m coordination zone is established upstream of the merging point. All vehicles are allowed to travel freely for 900 m to simulate realistic driving behaviors. We use the average travel time and average speed of vehicles within the coordination zone as the primary performance metrics. HDVs follow the classic intelligent

driver model (IDM) [38].

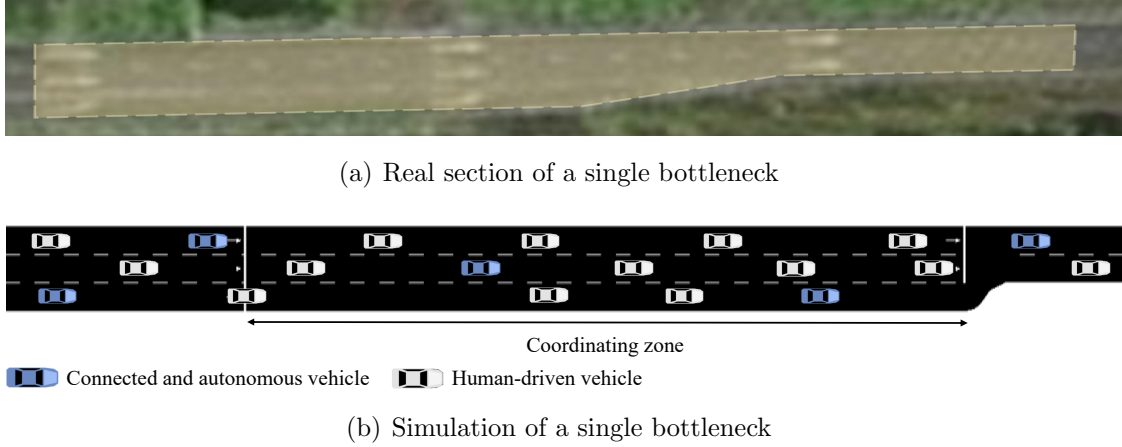


Figure 3: A single bottleneck section on the Hujin Highway.

To emulate a high-density traffic flow environment, vehicles are released onto the experimental section shown in Fig. 3(b) with an initial flow rate of 2000 veh/h . The lanes of these vehicles are random, and the CAV penetration rate is 15%. The coordination zone is spatially divided into multiple interconnected cells, each with a length of 300 m . The state and control action weight matrices for each CAV i are denoted as $Q_i = \text{diag}(0.5, 0.5, \dots, 0.5) \in \mathbb{R}^{(J+1) \times (J+1)}$ and $R_i = \text{diag}(1.0, 1.0, \dots, 1.0) \in \mathbb{R}^{(J+1) \times (J+1)}$, respectively. Other parameter settings are shown in Table 2.

Table 2: Parameter settings for the experiment.

Parameters	Values
MPC prediction horizon N	7 s
System update interval Δt	1 s
Cell length Δx	300 m
Jam density R	0.12 veh/m
Free flow speed V	33.33 m/s
Minimum control speed u_{\min}	5 m/s
Maximum control speed u_{\max}	33.33 m/s
Total road length	3000 m
Constriction factor λ_i	0.6

5.2 Performance Comparison

We apply the multiagent truncated rollout method method for longitudinal coordination control of CAVs, and compare it with five commonly used methods:

- Without control: This approach serves as the baseline where all vehicles (including CAVs) follow the IDM in SUMO simulations, devoid of external control interventions.

- Multiagent proximal policy optimization (MAPPO): MAPPO is a typical multiagent algorithm in RL [45], which achieves stable learning and efficient cooperation of agents by implementing centralized learning and decentralized execution.
- Heterogeneous-agent proximal policy optimization (HAPPO): The method enhances MAPPO via agent-by-agent sequential decision-making [23], where each agent’s policy update incorporates preceding agents’ optimized strategies.
- Model predictive control (MPC): It optimizes the control sequence for a finite horizon and uses a feedback correction mechanism to correct the prediction error based on the predictive model, achieving optimal control of the system [46].
- Distributed model predictive control (DMPC): The approach decomposes the global system into decentralized subsystems, each of which is governed by a separate MPC controller to reduce computational complexity [15].

As shown in Table 3, the multiagent truncated rollout method successfully improves both the average travel time and average speed of vehicles, due to its accurate modeling of global dynamics and agent-by-agent sequential decision-making. Compared to the without control scenario, the average travel time of vehicles on the road decreases by 17.29%, while the average speed increases by 19.42%.

Table 3: Performance comparisons of different approaches.

Approach	Average travel time	Average speed
Without control	191.54 <i>s</i>	11.43 <i>m/s</i>
MAPPO	169.95 <i>s</i> (↓ 11.27%)	12.75 <i>m/s</i> (↑ 11.55%)
HAPPO	168.39 <i>s</i> (↓ 12.09%)	12.90 <i>m/s</i> (↑ 12.86%)
MPC	165.94 <i>s</i> (↓ 13.37%)	13.14 <i>m/s</i> (↑ 14.96%)
DMPC	166.20 <i>s</i> (↓ 13.23%)	13.05 <i>m/s</i> (↑ 14.17%)
Our approach	158.43 <i>s</i> (↓ 17.29%)	13.65 <i>m/s</i> (↑ 19.42%)

These results also reveal that, compared to the conventional MAPPO algorithm in multi-agent reinforcement learning frameworks, the sequential decision-making mechanism enables the HAPPO algorithm to operate in a more stationary environment during training, thereby achieving superior control performance. However, the effectiveness of coordination strategies in MARL methods heavily relies on the agent population size predefined during training. When the number of agents dynamically changes, such methods often require retraining the network architecture, making them unsuitable for real-time control. As a result, in our simulation environment, the control performance of RL-based methods is inferior to that of MPC-based approaches. Although centralized MPC can theoretically achieve globally optimal performance, its practical application in large-scale multiagent systems faces two major limitations. First, as the number of CAVs increases, the optimization problem becomes highly non-convex and high-dimensional, making it extremely challenging to obtain high-quality solutions within constrained timeframes. Second, in our simulations, the centralized MPC solver frequently converges to local optima. These limitations directly result in its average travel time reduction of merely 13.37%. The DMPC method, while using distributed

control to reduce the average travel time to 13.23%, suffers from significant performance degradation due to the delayed transmission of control information during the iterative optimization process, resulting in a 4.06% worse outcome compared to the multiagent truncated rollout method.

5.3 Sensitivity Analysis

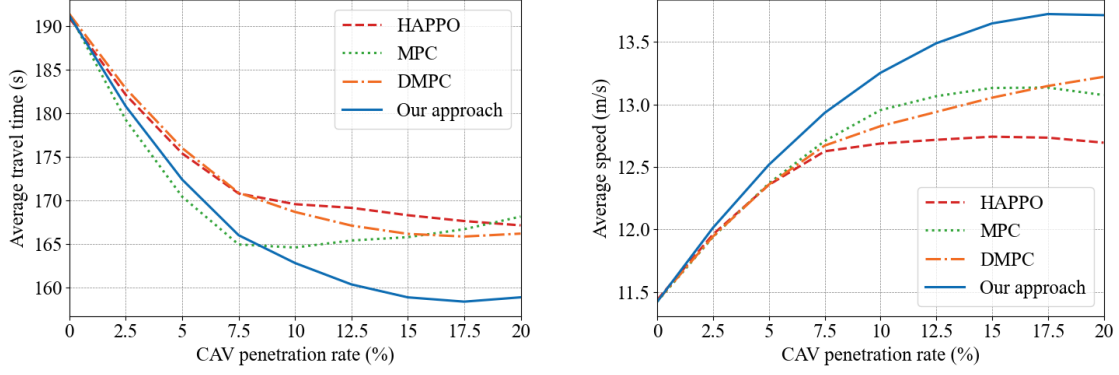
In this section, we explore the sensitivity of the proposed method to two key parameters: CAV penetration rate and coordination zone length, using the scenario in Fig. 3.

5.3.1 CAV Penetration Rate

We first conclude the impact of CAV penetration rate on average travel time and average speed. As shown in Fig. 4(a), with increasing CAV penetration, the average travel time for each method decreases. In particular, at low penetration rates (below 8%), MPC outperforms others due to its precise solving capability for small-scale optimization problems. But when the penetration rate exceeds 10%, the dimensionality and coupling complexity of the optimization problem increase rapidly, making the centralized MPC more prone to being trapped in local optima and less likely to obtain high-quality solutions within an acceptable computation time. As a result, its control performance degrades significantly. Although DMPC benefits increasingly from distributed control advantages at high penetrations, its local optimization features fundamentally limit overall effectiveness, reducing the average travel time by only approximately 13.4%. The HAPPO algorithm underperforms when confronting uncertainties in multiagent environments for convergence difficulties. These characteristics are also evidenced in Fig. 4(b). When CAV penetration rate surpasses 15%, the complexity of cooperative interactions leads to declining average speeds for HAPPO and MPC methods. In contrast, the multiagent truncated rollout method exhibits excellent advantages under high penetration scenarios, achieving over 17% reduction in average travel time and over 19% improvement in average speed. Additionally, it is worth noting that the control benefits of CAVs approach saturation when penetration reaches around 15%. This phenomenon may provide recommendations for traffic management, that prioritizing CAV deployment to approximately 15% in traffic bottleneck areas could balance cooperative control benefits with implementation costs.

5.3.2 Coordination Zone Length

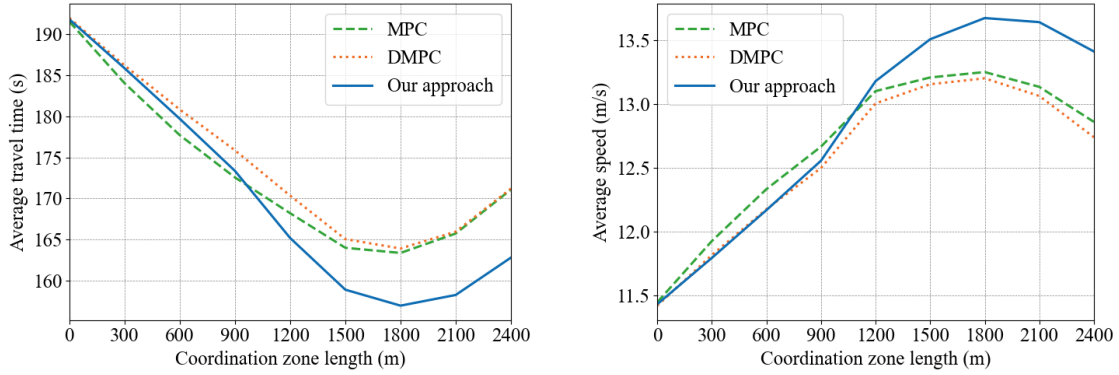
We then analyze how coordination zone length affects system performance. Fig. 5 shows that as the coordination zone expands from 300 m to 2400 m , the average travel time of all methods first decreases and then increases. This can be attributed to the dual impact of the coordination area on the collaboration capability and optimization complexity of CAVs. When the coordination zone is relatively short, the action space for CAVs is limited, and their collaboration potential is underutilized. As the coordination area expands, CAVs are able to coordinate over a larger range, improving overall traffic efficiency, with a reduction in average travel time of up to 18%. However, when the coordination area exceeds 1800 m , the increase in environmental information perceived by vehicles enhances decision-making



(a) Average travel time with the penetration rate (b) Average speed with the penetration rate

Figure 4: Sensitivity analysis of CAV penetration rate impact on system performance.

foresight but significantly escalates the computational and coordination difficulty of the optimization problem, leading to an increase in average travel time. By further comparing the performance of different control methods, we can observe that the multiagent truncated rollout method performs slightly worse than the MPC method in short coordination zones but is superior to the DMPC method. In large coordination areas (over 900 m), the proposed method exhibits superior performance, achieving lower average travel times than the MPC method. This indicates that it is more adaptable to large-scale systems.



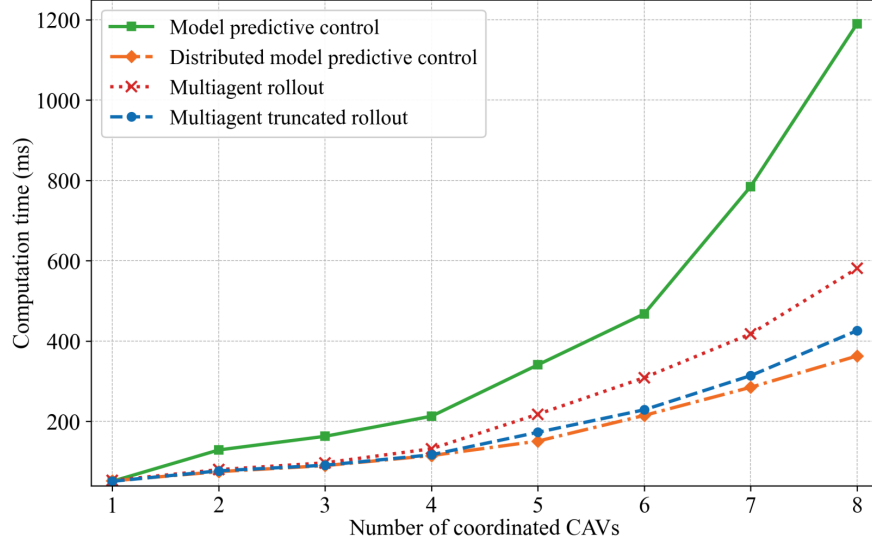
(a) Average travel time with the zone length (b) Average speed with the zone length

Figure 5: Sensitivity analysis of coordination zone length impact on system performance.

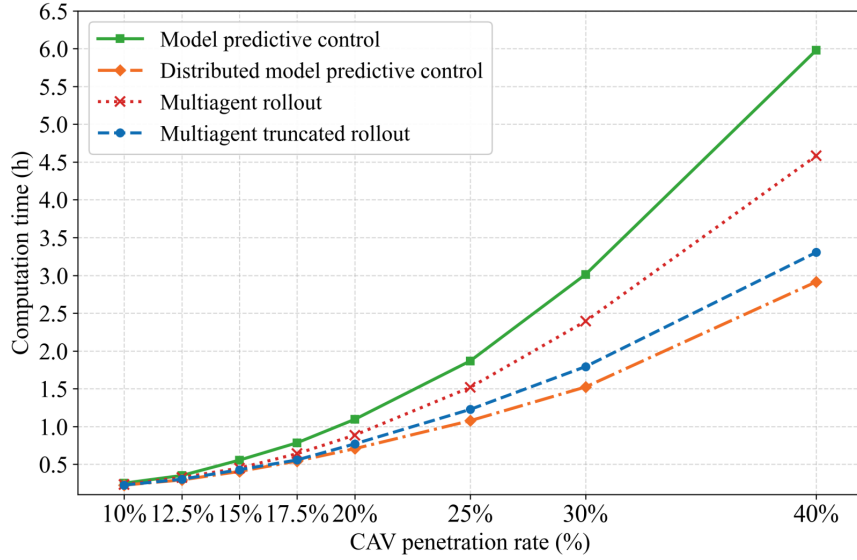
5.4 Scalability Analysis

To evaluate the scalability of the multiagent truncated rollout method in large-scale scenarios, we design a series of extended experiments within the 2100 m control zone scenario (Section 5.1), focusing on the computation time under varying numbers of CAVs. In addition to the benchmark MPC and DMPC methods, we also construct a standard multiagent

rollout approach for comparison. While employing a similar distributed control framework with agent-by-agent sequential decision-making, this baseline method fundamentally differs in horizon management: it utilizes a fixed prediction horizon ($N = 7$) for optimal control sequence computation, establishing a critical distinction from the dynamic truncation mechanism of our proposed approach.



(a) Single time step computation time



(b) Total system computation time

Figure 6: Computational scalability of control methods.

We first vary the number of CAVs from 1 to 8 in an identical traffic scenario and record the average single-step coordination time for each method. Then, with the simulation duration set to 1000 s, we test the total computation time required under CAV penetration rates ranging from 10% to 40%, aiming to comprehensively validate the computational efficiency of

the proposed approach. As Fig. 6 illustrates, the computational cost of all methods increases with the number of CAVs, though significant differences exist among the algorithms.

Traditional MPC faces severe computational bottlenecks when simultaneously optimizing the coordination of numerous CAVs, resulting in the steepest increase in solution time as the number of CAVs rises. While the standard multiagent rollout method incurs higher time costs than DMPC due to its sequential optimization diminishing the computational advantage of distributed frameworks, the truncated rollout mechanism reduces the dimensionality of decision variables at each step, offering a feasible solution for real-time control in high CAV penetration systems. Crucially, sensitivity testing on CAV penetration rates (Section 5.3.1) reveals that traffic flow regulation benefits essentially saturate when the overall CAV penetration rate reaches approximately 15%. Further increases in penetration lead to only marginal improvements in system performance. Under these conditions, the multiagent truncated rollout method reduces overall system computation time by 22.9% compared to the MPC approach, while maintaining computational costs only 5.7% higher than the DMPC method. And the proposed method achieves superior control performance relative to baseline methods. These findings confirm that, with a reasonable CAV penetration level, the proposed method maintains excellent performance and high computational efficiency within limited resources, effectively mitigating scalability concerns in practical deployment scenarios.

The computational efficiency improvement enabled by the truncated rollout mechanism is further validated across varying coordination zone lengths in the case study depicted in Fig. 3. As indicated by the red curve in Fig. 7, under a 15% CAV penetration rate, coordination zones shorter than 600 m yield only a 2% reduction in computation time compared to the standard rollout method. This is because the limited task scale minimizes the complexity difference between the two approaches. However, as the coordination zone expands, the efficiency gains from truncated optimization become significantly more pronounced. When the length of the coordination zone exceeds 2400 m , the total computation time of the system can be reduced by more than 10%.

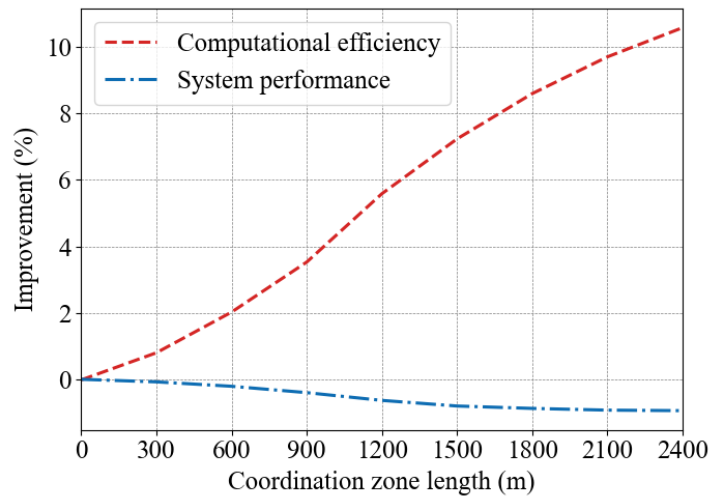


Figure 7: Improvement in computational efficiency and system performance.

Although truncated rollout delivers substantial efficiency improvements, partial horizon truncation induces marginal control performance degradation compared with standard rollout methods. However, as shown by the blue curve in Fig. 7, this performance gap remains below 1%. For instance, within the optimal control zone of 1800 m , the average travel time obtained using the truncated rollout method is 157.01 s , whereas the standard rollout method yields 155.65 s , representing a difference of approximately 1.36 s (0.87%). Given the over 8% improvement in computation time, this minor performance compromise is generally deemed acceptable.

6 Concluding Remarks

This paper proposes a novel multiagent truncated rollout method for optimizing highway traffic flow in mixed autonomy, with a specific focus on congested bottleneck scenarios. Firstly, based on a coupled PDE-ODE model that simultaneously captures the macroscopic evolution of traffic flow and the microscopic behavior of vehicles, we establish a road density state transition equation providing a unified description of road cell dynamics both with and without CAV influence. Subsequently, by treating each CAV as an independent controller, a distributed coordination framework is constructed. In contrast to traditional distributed model predictive control approach that rely on parallel optimization, our architecture introduces an agent-by-agent sequential optimization mechanism. This allows each CAV to make decisions in turn based on information from its neighbors, thereby explicitly enhancing coordination among CAVs. Additionally, our approach incorporates a truncated rollout technique that evaluates solution quality using upper and lower bounds of the objective function and adaptively truncates the optimization horizon to reduce computational cost. Theoretical analysis shows that the proposed method not only guarantees input-to-state stability for each CAV subsystem and achieves lower computational complexity, but also ensures monotonic improvement of the system-level objective function across iterations. Simulation experiments conducted on a real-world bottleneck scenario of Shanghai Hujin Expressway demonstrate that the multiagent truncated rollout method effectively reduces vehicle travel time. Furthermore, compared to traditional model predictive control and distributed model predictive control approaches, the proposed method achieves a superior balance between performance enhancement and scalability in large-scale systems.

This work can be extended in several important directions. First, incorporating lane changing behaviors can enable the joint optimization of longitudinal and lateral control. This allows for a more realistic representation of driving dynamics in real-world. Second, the impact of various uncertainties on control performance, including sensor noise, communication delays, and the unpredictable behaviors of human-driven vehicles, will be analyzed. By introducing robust optimization techniques or learning-based adaptive mechanisms, the stability and reliability of the proposed method can be enhanced. Finally, the control framework can be extended to larger and more complex networks by designing spatially distributed multiagent coordination mechanisms across multiple bottlenecks.

Appendix

Appendix A Derivation of the Density Transfer Equation

Cells Without Controlled CAVs

In road cells without controlled CAVs, the calculation of density follows Eq. 4. We organize it as,

$$\rho_j^{k+1} = \rho_j^k + f_1(\rho_{j-1}^k, \rho_j^k, \rho_{j+1}^k),$$

where the nonlinear function $f_1(\rho_{j-1}^k, \rho_j^k, \rho_{j+1}^k)$ is derived from Eqs. (4b)-(4e),

$$\begin{aligned} f_1(\rho_{j-1}^k, \rho_j^k, \rho_{j+1}^k) = & -\frac{\Delta t}{\Delta x} \left[\min \{ f(\min \{ \rho_j^k, \rho_* \}), f(\max \{ \rho_{j+1}^k, \rho_* \}) \} \right. \\ & \left. - \min \{ f(\min \{ \rho_{j-1}^k, \rho_* \}), f(\max \{ \rho_j^k, \rho_* \}) \} \right] \end{aligned}$$

Cells with Controlled CAVs

If the action u_i of CAV i does not satisfy constraint (3c), we reconstruct the upstream density $\hat{\rho}_{j-\frac{1}{2}}^k(u_i)$ and downstream density $\check{\rho}_{j+\frac{1}{2}}^k(u_i)$ of the cell j in which this CAV is located by solving the following equation,

$$\frac{\alpha R}{4V}(V - u_i)^2 = V\rho(u_i) \left(1 - \frac{\rho(u_i)}{R} \right) - u_i\rho(u_i).$$

Then,

$$\begin{aligned} \hat{\rho}_{j-\frac{1}{2}}^k(u_i) &= R(V - u_i) \frac{1 + \sqrt{1 - \alpha}}{2V}, \\ \check{\rho}_{j+\frac{1}{2}}^k(u_i) &= R(V - u_i) \frac{1 - \sqrt{1 - \alpha}}{2V}. \end{aligned}$$

For $F_{j+\frac{1}{2}}^k$ in Eq. 6,

(i) If $\Delta t_i^k \leq \Delta t$,

$$\begin{aligned} F_{j+\frac{1}{2}}^k &= \frac{\Delta t_i^k}{\Delta t} f(\check{\rho}_{j+\frac{1}{2}}^k(u_i)) + \left(1 - \frac{\Delta t_i^k}{\Delta t} \right) f(\hat{\rho}_{j-\frac{1}{2}}^k(u_i)) \\ &= \frac{\Delta t_i^k}{\Delta t} \left[f(\check{\rho}_{j+\frac{1}{2}}^k(u_i)) - f(\hat{\rho}_{j-\frac{1}{2}}^k(u_i)) \right] + f(\hat{\rho}_{j-\frac{1}{2}}^k(u_i)). \end{aligned}$$

Since,

$$\Delta t_i^k = \frac{1 - d_i^k}{u_i^k} \Delta x, \quad d_i^k = \frac{\rho_j^k - \hat{\rho}_{j-\frac{1}{2}}^k(u_i)}{\check{\rho}_{j+\frac{1}{2}}^k(u_i) - \hat{\rho}_{j-\frac{1}{2}}^k(u_i)},$$

we can get,

$$\begin{aligned}
& \frac{\Delta t_i^k}{\Delta t} \left[f \left(\check{\rho}_{j+\frac{1}{2}}^k(u_i) \right) - f \left(\hat{\rho}_{j-\frac{1}{2}}^k(u_i) \right) \right] \\
&= \frac{\Delta t_i^k}{\Delta t} \left[V \check{\rho}_{j+\frac{1}{2}}^k(u_i) \left(1 - \frac{\check{\rho}_{j+\frac{1}{2}}^k(u_i)}{R} \right) - V \hat{\rho}_{j-\frac{1}{2}}^k(u_i) \left(1 - \frac{\hat{\rho}_{j-\frac{1}{2}}^k(u_i)}{R} \right) \right] \\
&= \frac{1 - d_i^k}{u_i^k} \frac{\Delta x}{\Delta t} \left[V \check{\rho}_{j+\frac{1}{2}}^k(u_i) \left(1 - \frac{\check{\rho}_{j+\frac{1}{2}}^k(u_i)}{R} \right) - V \hat{\rho}_{j-\frac{1}{2}}^k(u_i) \left(1 - \frac{\hat{\rho}_{j-\frac{1}{2}}^k(u_i)}{R} \right) \right] \\
&= \frac{\check{\rho}_{j+\frac{1}{2}}^k(u_i) - \rho_j^k}{\check{\rho}_{j+\frac{1}{2}}^k(u_i) - \hat{\rho}_{j-\frac{1}{2}}^k(u_i)} \frac{\Delta x}{u_i^k \Delta t} \left[V \check{\rho}_{j+\frac{1}{2}}^k(u_i) \left(1 - \frac{\check{\rho}_{j+\frac{1}{2}}^k(u_i)}{R} \right) - V \hat{\rho}_{j-\frac{1}{2}}^k(u_i) \left(1 - \frac{\hat{\rho}_{j-\frac{1}{2}}^k(u_i)}{R} \right) \right] \\
&= \frac{\Delta x}{u_i^k \Delta t} \left[u_i \left(\check{\rho}_{j+\frac{1}{2}}^k(u_i) - \rho_j^k \right) \right],
\end{aligned}$$

so,

$$F_{j+\frac{1}{2}}^k = \frac{\Delta x}{\Delta t} \left(\check{\rho}_{j+\frac{1}{2}}^k(u_i) - \rho_j^k \right) + f \left(\hat{\rho}_{j-\frac{1}{2}}^k(u_i) \right).$$

(ii) If $\Delta t_i^k > \Delta t$,

$$F_{j+\frac{1}{2}}^k = f \left(\check{\rho}_{j+\frac{1}{2}}^k(u_i) \right).$$

For $F_{j-\frac{1}{2}}^k$ in Eq. 5,

(i) If $\rho_{j-1}^k \leq \rho_*$ and $\hat{\rho}_{j-\frac{1}{2}}^k(u_i) \leq \rho_*$,

$$\begin{aligned}
D(\rho_{j-1}^k) &= f(\min\{\rho_{j-1}^k, \rho_*\}) = f(\rho_{j-1}^k), \\
S(\hat{\rho}_{j-\frac{1}{2}}^k(u_i)) &= f(\max\{\hat{\rho}_{j-\frac{1}{2}}^k(u_i), \rho_*\}) = f(\rho_*), \\
F_{j-\frac{1}{2}}^k &= \min\{D(\rho_{j-1}^k), S(\hat{\rho}_{j-\frac{1}{2}}^k(u_i))\} = f(\rho_{j-1}^k).
\end{aligned}$$

(ii) If $\rho_{j-1}^k \leq \rho_*$ and $\hat{\rho}_{j-\frac{1}{2}}^k(u_i) > \rho_*$,

$$\begin{aligned}
D(\rho_{j-1}^k) &= f(\min\{\rho_{j-1}^k, \rho_*\}) = f(\rho_{j-1}^k), \\
S(\hat{\rho}_{j-\frac{1}{2}}^k(u_i)) &= f(\max\{\hat{\rho}_{j-\frac{1}{2}}^k(u_i), \rho_*\}) = f(\hat{\rho}_{j-\frac{1}{2}}^k(u_i)), \\
F_{j-\frac{1}{2}}^k &= \min\{D(\rho_{j-1}^k), S(\hat{\rho}_{j-\frac{1}{2}}^k(u_i))\} = \min\{f(\rho_{j-1}^k), f(\hat{\rho}_{j-\frac{1}{2}}^k(u_i))\}.
\end{aligned}$$

(iii) If $\rho_{j-1}^k > \rho_*$ and $\hat{\rho}_{j-\frac{1}{2}}^k(u_i) \leq \rho_*$,

$$\begin{aligned}
D(\rho_{j-1}^k) &= f(\min\{\rho_{j-1}^k, \rho_*\}) = f(\rho_*), \\
S(\hat{\rho}_{j-\frac{1}{2}}^k(u_i)) &= f(\max\{\hat{\rho}_{j-\frac{1}{2}}^k(u_i), \rho_*\}) = f(\rho_*), \\
F_{j-\frac{1}{2}}^k &= \min\{D(\rho_{j-1}^k), S(\hat{\rho}_{j-\frac{1}{2}}^k(u_i))\} = f(\rho_*).
\end{aligned}$$

(iv) If $\rho_{j-1}^k > \rho_*$ and $\hat{\rho}_{j-\frac{1}{2}}^k(u_i) > \rho_*$,

$$\begin{aligned} D(\rho_{j-1}^k) &= f(\min\{\rho_{j-1}^k, \rho_*\}) = f(\rho_*), \\ S(\hat{\rho}_{j-\frac{1}{2}}^k(u_i)) &= f(\max\{\hat{\rho}_{j-\frac{1}{2}}^k(u_i), \rho_*\}) = f(\hat{\rho}_{j-\frac{1}{2}}^k(u_i)), \\ F_{j-\frac{1}{2}}^k &= \min\{D(\rho_{j-1}^k), S(\hat{\rho}_{j-\frac{1}{2}}^k(u_i))\} = f(\hat{\rho}_{j-\frac{1}{2}}^k(u_i)). \end{aligned}$$

Above all, the density state transfer equation for a road cell containing a controlled CAV can be expressed as follows,

$$\begin{aligned} \rho_j^{k+1} &= \rho_j^k - \frac{\Delta t}{\Delta x} (F_{j+\frac{1}{2}}^k - F_{j-\frac{1}{2}}^k) \\ &= \rho_j^k + d\rho_j^k + [bc + a(1-b)c] \frac{\Delta t}{\Delta x} f(\rho_{j-1}^k) + b(1-c) \frac{\Delta t}{\Delta x} f(\rho_*) \\ &\quad + [ac(1-b)(1-2d) - bd + (1-b)(1-c)(1-d)] \frac{\Delta t}{\Delta x} f(\hat{\rho}_{j-\frac{1}{2}}^k(u_i)) \\ &\quad - d\check{\rho}_{j+\frac{1}{2}}^k(u_i) - (1-d) \frac{\Delta t}{\Delta x} f(\check{\rho}_{j+\frac{1}{2}}^k(u_i)), \end{aligned}$$

where a, b, c, d are all Heaviside functions,

$$\begin{aligned} a &= \begin{cases} 1, & f(\rho_{j-1}^k) \leq f(\hat{\rho}_{j-\frac{1}{2}}^k(u_i)), \\ 0, & f(\rho_{j-1}^k) > f(\hat{\rho}_{j-\frac{1}{2}}^k(u_i)), \end{cases} & b &= \begin{cases} 1, & \hat{\rho}_{j-\frac{1}{2}}^k(u_i) \leq \rho_*, \\ 0, & \hat{\rho}_{j-\frac{1}{2}}^k(u_i) > \rho_*, \end{cases} \\ c &= \begin{cases} 1, & \rho_{j-1}^k \leq \rho_*, \\ 0, & \rho_{j-1}^k > \rho_*, \end{cases} & d &= \begin{cases} 1, & \Delta t_i^k \leq \Delta t, \\ 0, & \Delta t_i^k > \Delta t. \end{cases} \end{aligned}$$

Then the nonlinear functions $f_2(\rho_{j-1}^k, \rho_j^k)$ and $f_3(u_i)$ are,

$$\begin{aligned} f_2(\rho_{j-1}^k, \rho_j^k) &= d\rho_j^k + [bc + a(1-b)c] \frac{\Delta t}{\Delta x} f(\rho_{j-1}^k) + b(1-c) \frac{\Delta t}{\Delta x} f(\rho_*), \\ f_3(u_i) &= [ac(1-b)(1-2d) - bd + (1-b)(1-c)(1-d)] \frac{\Delta t}{\Delta x} f(\hat{\rho}_{j-\frac{1}{2}}^k(u_i)) \\ &\quad - d\check{\rho}_{j+\frac{1}{2}}^k(u_i) - (1-d) \frac{\Delta t}{\Delta x} f(\check{\rho}_{j+\frac{1}{2}}^k(u_i)). \end{aligned}$$

Appendix B Derivation of Action Range Violating Eq. (3c)

At any time step k , for the action u_i of CAV $i \in I^k$ not to satisfy constraint (3c), there must be $u_i > v(\rho_j^k)$ and the following inequality holds,

$$\begin{aligned} &f(\rho_j^k) - u_i \rho_j^k - \frac{\alpha R}{4V} (V - u_i)^2 \\ &= V \rho_j^k \left(1 - \frac{\rho_j^k}{R}\right) - u_i \rho_j^k - \frac{\alpha R}{4V} (V - u_i)^2 \end{aligned}$$

$$>0,$$

i.e.,

$$\begin{aligned} & -V\rho_j^k \left(1 - \frac{\rho_j^k}{R}\right) + u_i \rho_j^k + \frac{\alpha R}{4V}(V - u_i)^2 \\ & = \frac{\alpha R}{4V} u_i^2 - \left(\frac{\alpha R}{2} - \rho_j^k\right) u_i - \left(V\rho_j^k - \frac{V\rho_j^{k2}}{R} - \frac{\alpha RV}{4}\right) \\ & < 0, \end{aligned}$$

where ρ_j^k denotes the density of cell j where cav i is located.

The roots of the quadratic function $\frac{\alpha R}{4V} u_i^2 - \left(\frac{\alpha R}{2} - \rho_j^k\right) u_i - \left(V\rho_j^k - \frac{V\rho_j^{k2}}{R} - \frac{\alpha RV}{4}\right) = 0$ are,

$$\gamma_1(\rho_j^k) = V - \frac{2V\rho_j^k}{\alpha R} (1 + \sqrt{1 - \alpha}), \quad \gamma_2(\rho_j^k) = V - \frac{2V\rho_j^k}{\alpha R} (1 - \sqrt{1 - \alpha}).$$

where $\gamma_2(\rho_j^k)$ must be less than $v(\rho_j^k)$. This is because if $\gamma_2(\rho_j^k) \leq v(\rho_j^k)$ and $\alpha = \frac{W-1}{W}$, there must be

$$\frac{2}{\alpha} (1 - \sqrt{1 - \alpha}) = \frac{2W - 2\sqrt{W}}{W - 1} \leq 1,$$

then $W = 1$. This is inconsistent with the assumption that the number of lanes upstream of the merge point is $W > 1$.

Since $\frac{\alpha R}{4V} > 0$, the solution set of the inequality is,

$$\gamma_1(\rho_j^k) \leq u_i \leq \gamma_2(\rho_j^k).$$

References

- [1] Anupriya, Prateek Bansal, and Daniel J. Graham. Congestion in cities: Can road capacity expansions provide a solution? *Transportation Research Part A: Policy and Practice*, 174:103726, 2023.
- [2] Jingjing Bao, Celimuge Wu, Yangfei Lin, Lei Zhong, Xianfu Chen, and Rui Yin. A scalable approach to optimize traffic signal control with federated reinforcement learning. *Scientific Reports*, 13:19184, 2023.
- [3] Dimitri P. Bertsekas. Constrained multiagent rollout and multidimensional assignment with the auction algorithm. *ArXiv*, abs/2002.07407, 2020.
- [4] Dimitri P. Bertsekas. Multiagent reinforcement learning: Rollout and policy iteration. *IEEE/CAA Journal of Automatica Sinica*, 8(2):249–272, 2021.
- [5] Dimitri P. Bertsekas, John N. Tsitsiklis, and Cynara Wu. Rollout algorithms for combinatorial optimization. *Journal of Heuristics*, 3:245–262, 1997.

- [6] Dimitri Panteli Bertsekas. Multiagent rollout algorithms and reinforcement learning. *ArXiv*, abs/1910.00120, 2019.
- [7] Sushmita Bhattacharya, Siva Kailas, Sahil Badyal, Stephanie Gil, and Dimitri P. Bertsekas. Multiagent reinforcement learning: Rollout and policy iteration for pomdp with application to multirobot problems. *IEEE Transactions on Robotics*, 40:2003–2023, 2024.
- [8] Xiangdong Chen, Xi Lin, Qiang Meng, and Meng Li. Coordinated traffic control of urban networks with dynamic entrance holding for mixed cav traffic. *Transportation Research Part E: Logistics and Transportation Review*, 178:103264, 2023.
- [9] Koohong Chung, Jittichai Rudjanakanoknad, and Michael J. Cassidy. Relation between traffic density and capacity drop at three freeway bottlenecks. *Transportation Research Part B: Methodological*, 41(1):82–95, 2007.
- [10] Chiara Daini, Paola Goatin, Maria Laura Delle Monache, and Antonella Ferrara. Centralized traffic control via small fleets of connected and automated vehicles. In *2022 European Control Conference*, pages 371–376, 2022.
- [11] Chiara Daini, Maria Laura Delle Monache, Paola Goatin, and Antonella Ferrara. Traffic control via fleets of connected and automated vehicles. *IEEE Transactions on Intelligent Transportation Systems*, 26(2):1573–1582, 2025.
- [12] Ziluo Ding, Zeyuan Liu, Zhirui Fang, Kefan Su, Liwen Zhu, and Zongqing Lu. Multi-agent coordination via multi-level communication. In *Advances in Neural Information Processing Systems*, volume 37, pages 118513–118539, 2024.
- [13] Antonio Ferramosca, Daniel Limon, Ignacio Alvarado, Teodoro Alamo, and Eduardo F. Camacho. Mpc for tracking of constrained nonlinear systems. In *Proceedings of the 48th IEEE Conference on Decision and Control held jointly with 2009 28th Chinese Control Conference*, pages 7978–7983, 2009.
- [14] Zhibo Gao, Zhizhou Wu, Wei Hao, Keke Long, Young-Ji Byon, and Kejun Long. Optimal trajectory planning of connected and automated vehicles at on-ramp merging area. *IEEE Transactions on Intelligent Transportation Systems*, 23(8):12675–12687, 2022.
- [15] Nathan Goulet and Beshah Ayalew. Distributed maneuver planning with connected and automated vehicles for boosting traffic efficiency. *IEEE Transactions on Intelligent Transportation Systems*, 23(8):10887–10901, 2022.
- [16] Shaocheng Jia, Sze Chun Wong, and Wai Wong. Adaptive signal control at partially connected intersections: A stochastic optimization model for uncertain vehicle arrival rates. *Transportation Research Part B: Methodological*, 193:103161, 2025.
- [17] Wen-Long Jin. A kinematic wave theory of multi-commodity network traffic flow. *Transportation Research Part B: Methodological*, 46(8):1000–1022, 2012.

- [18] John H. Kodi, Emmanuel Kidando, Priyanka Alluri, and Thobias Sando. Guidelines for activating ramp metering signals in response to non-recurrent congestion during off-peak hours using a statistical method. *Transportation Research Record*, 2678(12):1237–1251, 2024.
- [19] Jakub Grudzien Kuba, Muning Wen, Linghui Meng, shangding gu, Haifeng Zhang, David Mguni, Jun Wang, and Yaodong Yang. Settling the variance of multi-agent policy gradients. In *Advances in Neural Information Processing Systems*, volume 34, pages 13458–13470, 2021.
- [20] Jia Li, Di Chen, and Michael Zhang. Equilibrium modeling of mixed autonomy traffic flow based on game theory. *Transportation Research Part B: Methodological*, 166:110–127, 2022.
- [21] Mengjie Li, Haoning Xi, Chi Xie, Zuo-Jun Max Shen, and Yifan Hu. Real-time vehicle relocation, personnel dispatch and trip pricing for carsharing systems under supply and demand uncertainties. *Transportation Research Part B: Methodological*, 193:103154, 2025.
- [22] Thibault Liard, Raphael Stern, and Maria Laura Delle Monache. A pde-ode model for traffic control with autonomous vehicles. *Networks and Heterogeneous Media*, 18(3):1190–1206, 2023.
- [23] Lu Liu, Maonan Wang, Man-On Pun, and Xi Xiong. A multi-agent rollout approach for highway bottleneck decongestion in mixed autonomy. In *2024 IEEE 27th International Conference on Intelligent Transportation Systems*, pages 3377–3382, 2024.
- [24] Shuai Liu, Anna Sadowska, and Bart De Schutter. A scenario-based distributed model predictive control approach for freeway networks. *Transportation Research Part C: Emerging Technologies*, 136:103261, 2022.
- [25] Pablo Alvarez Lopez, Michael Behrisch, Laura Bieker-Walz, Jakob Erdmann, Yun-Pang Flötteröd, Robert Hilbrich, Leonhard Lücken, Johannes Rummel, Peter Wagner, and Evamarie Wiessner. Microscopic traffic simulation using sumo. In *2018 IEEE 21st International Conference on Intelligent Transportation Systems*, pages 2575–2582, 2018.
- [26] Gongyuan Lu, Zili Shen, Xiaobo Liu, Yu (Marco) Nie, and Zhiqiang Xiong. Are autonomous vehicles better off without signals at intersections? a comparative computational study. *Transportation Research Part B: Methodological*, 155:26–46, 2022.
- [27] Anna Lukina, Lukas Esterle, Christian Hirsch, Ezio Bartocci, Junxing Yang, Ashish Tiwari, Scott A. Smolka, and Radu Grosu. Ares: Adaptive receding-horizon synthesis of optimal plans. In *Tools and Algorithms for the Construction and Analysis of Systems*, pages 286–302, Berlin, Heidelberg, 2017. Springer Berlin Heidelberg.
- [28] Jie Luo, Defeng He, Wei Zhu, and Haiping Du. Multiobjective platooning of connected and automated vehicles using distributed economic model predictive control. *IEEE Transactions on Intelligent Transportation Systems*, 23(10):19121–19135, 2022.

- [29] Muting Ma and Zhixia Li. A speed-maximization trajectory optimization model on a reservation-based intersection control system. *Transportation Research Part C: Emerging Technologies*, 154:104266, 2023.
- [30] Lalo Magni, Davide Raimondo, and Riccardo Scattolini. Regional input-to-state stability for nonlinear model predictive control. *IEEE Transactions on Automatic Control*, 51(9):1548–1553, 2006.
- [31] Wendi Nie, Yonghong You, Victor Chung-Sing Lee, and Yaoxin Duan. Variable speed limit control for individual vehicles on freeway bottlenecks with mixed human and automated traffic flows. In *2021 IEEE 24th International Conference on Intelligent Transportation Systems*, pages 2492–2498, 2021.
- [32] Ioannis A. Ntousakis, Ioannis K. Nikolos, and Markos Papageorgiou. Optimal vehicle trajectory planning in the context of cooperative merging on highways. *Transportation Research Part C: Emerging Technologies*, 71:464–488, 2016.
- [33] Giulia Piacentini, Paola Goatin, and Antonella Ferrara. Traffic control via platoons of intelligent vehicles for saving fuel consumption in freeway systems. *IEEE Control Systems Letters*, 5(2):593–598, 2021.
- [34] Yanyan Qin, Hao Wang, and Daiheng Ni. Lighthill-whitham-richards model for traffic flow mixed with cooperative adaptive cruise control vehicles. *Transportation science*, (4):55, 2021.
- [35] Jiahua Qiu and Lili Du. Cooperative trajectory control for synchronizing the movement of two connected and autonomous vehicles separated in a mixed traffic flow. *Transportation Research Part B: Methodological*, 174:102769, 2023.
- [36] Paul I. Richards. Shock waves on the highway. *Operations Research*, 4(1):42–51, 1956.
- [37] András Sasfi, Melanie N. Zeilinger, and Johannes Köhler. Robust adaptive mpc using control contraction metrics. *Automatica*, 155:111169, 2023.
- [38] Jie Sun, Zuduo Zheng, and Jian Sun. Stability analysis methods and their applicability to car-following models in conventional and connected environments. *Transportation Research Part B: Methodological*, 109:212–237, 2018.
- [39] Eugene Vinitsky, Nathan Lichtlé, Kanaad Parvate, and Alexandre Bayen. Optimizing mixed autonomy traffic flow with decentralized autonomous vehicles and multi-agent reinforcement learning. *ACM Transactions on Cyber-Physical Systems*, 7(2), 2023.
- [40] Junyang Wang, Haiyang Xu, Haitao Jia, Xi Zhang, Ming Yan, Weizhou Shen, Ji Zhang, Fei Huang, and Jitao Sang. Mobile-agent-v2: Mobile device operation assistant with effective navigation via multi-agent collaboration. In *Advances in Neural Information Processing Systems*, volume 37, pages 2686–2710, 2024.

- [41] Ning Wang, Xiao Chen, and Jonas Mårtensson. Rollout-based interactive motion planning for automated vehicles. In *2023 IEEE 26th International Conference on Intelligent Transportation Systems*, pages 4187–4194, 2023.
- [42] Muning Wen, Jakub Kuba, Runji Lin, Weinan Zhang, Ying Wen, Jun Wang, and Yaodong Yang. Multi-agent reinforcement learning is a sequence modeling problem. In *Advances in Neural Information Processing Systems*, volume 35, pages 16509–16521, 2022.
- [43] Xi Xiong, Junyi Sha, and Li Jin. Optimizing coordinated vehicle platooning: An analytical approach based on stochastic dynamic programming. *Transportation Research Part B: Methodological*, 150:482–502, 2021.
- [44] Yongjie Xue, Li Zhang, Yuxuan Sun, Yu Zhou, Zhiyuan Liu, and Bin Yu. Conflict-free optimal control of connected automated vehicles at unsignalized intersections: A condition-based computational framework with constrained terminal position and speed. *Transportation Research Part B: Methodological*, 195:103209, 2025.
- [45] Chao Yu, Akash Velu, Eugene Vinitsky, Yu Wang, Alexandre M. Bayen, and Yi Wu. The surprising effectiveness of mappo in cooperative, multi-agent games. *ArXiv*, abs/2103.01955, 2021.
- [46] Hanyu Zhang and Lili Du. Platoon-centered control for eco-driving at signalized intersection built upon hybrid mpc system, online learning and distributed optimization part ii: Theoretical analysis. *Transportation Research Part B: Methodological*, 172:199–216, 2023.
- [47] Hongjun Michael Zhang. A finite difference approximation of a non-equilibrium traffic flow model. *Transportation Research Part B: Methodological*, 35(4):337–365, 2001.
- [48] Liguozhang, Jiahao Wu, and Jingyuan Zhan. Adaptive observer design for coupled ode–hyperbolic pde systems with application to traffic flow estimation. *Automatica*, 167:111796, 2024.
- [49] Yifan Zhong, Jakub Grudzien Kuba, Xidong Feng, Siyi Hu, Jiaming Ji, and Yaodong Yang. Heterogeneous-agent reinforcement learning. *Journal of Machine Learning Research*, 25(32):1–67, 2024.
- [50] Yang Zhou, Meng Wang, and Soyoung Ahn. Distributed model predictive control approach for cooperative car-following with guaranteed local and string stability. *Transportation Research Part B: Methodological*, 128:69–86, 2019.
- [51] Yang Zhou, Meng Wang, and Soyoung Ahn. Distributed model predictive control approach for cooperative car-following with guaranteed local and string stability. *Transportation Research Part B: Methodological*, 128:69–86, 2019.
- [52] Lian Zhu, Linjun Lu, Xianing Wang, Chenming Jiang, and Nanfei Ye. Operational characteristics of mixed-autonomy traffic flow on the freeway with on- and off-ramps

- and weaving sections: An rl-based approach. *IEEE Transactions on Intelligent Transportation Systems*, 23(8):13512–13525, 2022.
- [53] Yue Zu, Chenhui Liu, Ran Dai, Anuj Sharma, and Jing Dong. Real-time energy-efficient traffic control via convex optimization. *Transportation Research Part C: Emerging Technologies*, 92:119–136, 2018.
- [54] Mladen Čičić and Karl Henrik Johansson. Traffic regulation via individually controlled automated vehicles: a cell transmission model approach. In *2018 21st International Conference on Intelligent Transportation Systems*, pages 766–771, 2018.